


RESEARCH ARTICLE

WILEY

Loads assessment of a fixed-bottom offshore wind farm with wake steering

Kelsey Shaler¹  | Jason Jonkman¹ | Garrett E. Barter¹ | Jasper J. Kreeft² | Jelle P. Muller²

¹National Renewable Energy Laboratory, Golden, Colorado, USA

²Shell Global Solutions International B.V., The Hague, Netherlands

Correspondence

Kelsey Shaler, National Renewable Energy Laboratory, Golden, CO, USA.
Email: kelsey.shaler@nrel.gov

Abstract

Wake steering via deliberate yaw offset is an emerging wind farm control technique that has the potential to mitigate wake losses and further increase wind farm energy yield. The loads impact of this technique has been studied, but there is limited insight into wind-farm-wide impacts of wake steering. Understanding such impacts is crucial to determining the feasibility of using wake steering in commercial wind farms. To that end, this work investigates the impacts of wake steering on the loads of all turbine components across all turbines in a wind farm operating under a broad set of inflow conditions, including inflow velocity, shear exponent, turbulence class, and inflow angle. This was done by performing FAST.Farm simulations of a 12-turbine wind farm array, excerpted from a larger hypothetical wind farm. The International Energy Agency Wind 15-MW reference wind turbine was modeled atop a monopile substructure, an open-source model that closely approximates the properties of similar commercial options. Wake steering was included via yaw offsets that were computed using an offline optimization with the National Renewable Energy Laboratory tool FLORIS. For each inflow case, the 12-turbine array was simulated with and without wake steering. Results were compared in terms of time-averaged means, standard deviations, ultimate loads, and damage-equivalent loads. The findings show that because wake steering is generally applied at rated wind speeds and below, it is unlikely to drive ultimate loads. For fatigue loads, wake steering does increase the overall fatigue accumulation for some load channels, such as blade-root and shaft bending. This is to be expected when overall power yield increases but may cause the damage accumulation to be more uniform throughout the array. The significance of the added fatigue loading is dependent on how frequent wake steering is utilized in the overall set of inflow conditions across the wind rose.

KEYWORDS

FAST.Farm, turbine structural loads, turbine wakes, wake steering, wind farm

This is an open access article under the terms of the [Creative Commons Attribution-NonCommercial](https://creativecommons.org/licenses/by-nc/4.0/) License, which permits use, distribution and reproduction in any medium, provided the original work is properly cited and is not used for commercial purposes.

© 2022 The Authors. *Wind Energy* published by John Wiley & Sons Ltd.

1 | INTRODUCTION

New offshore wind projects exist in a competitive yet financially uncertain market. In the United States, the local supply chain is still evolving, leading to extensive cost uncertainty, yet projects must nevertheless make long-lead-time commitments. Concurrently, the competition of traditional coal and gas power with land-based wind and solar are continuously in flux. This market landscape puts tremendous pressure on developers to extract as much power yield (i.e., revenue) as possible from their turbines. Recent commercial turbine models with nameplate capacities in the range of 13–16 MW will enable high power capacity factors with low logistical cost per unit of energy delivered. In addition to larger wind turbines, new controls advancements are being developed, such as wake steering via controlled yaw offset, that offer the potential to mitigate wake losses and further increase wind farm energy yield. Wake steering in particular has been proven to recoup wake losses for some parts of the wind rose and increase net power yield in computational models,^{1–4} wind tunnel experiments,^{5–8} and field trials.^{9–12} The basic concept behind wake steering is that when the incoming flow angle aligns with rows/columns of a turbine array, the front-row turbine intentionally yaws away from the aligned flow to deflect its wake away from downstream turbines. This sacrifices some power output from the upstream turbine but significantly increases the power yield of the whole array. For deeper arrays, many turbines would operate with a yaw offset angle. The volume of published research on the topic is extensive, and discussion of all the nuances is beyond the scope of this work. A review article by Houk¹³ serves as a helpful summary and index of prior work.

Wake steering via intentional yaw offset represents a new approach to operating a turbine array with structural load profiles that differ from those rooted in decades of design and operational experience. Ultimate load envelopes impact turbine safety margins, and fatigue load envelopes impact turbine lifetime. Thus, new structural load profiles that could potentially exceed prior ultimate and fatigue load envelopes pose a risk to standards-based safety margins, project financing, and insurance agreements that underpin successful commercial wind projects. The potential impact of wake steering on turbine loads is a convoluted problem. By contrast, wakes are known to increase local turbulence intensity (TI) due to both wake meandering and wake-added turbulence,^{14,15} which is a strong driver of fatigue loading. Therefore, deflecting wakes away from downstream turbines could alleviate fatigue damage, especially on the blades. On the other hand, higher inflow velocity for the downstream turbines will increase thrust and torque loading cycles on the structure.

The loads impact from wake steering has been studied in model and experimental settings, typically with a narrow focus of two to three turbine arrays and a small subset of load channels. Past studies have focused on the loads impact of yaw offset on a turbine itself and partial waking on downstream turbines. Past studies on turbine yaw offset have suggested higher extreme and fatigue bending moments through the rotor and drivetrain, but with cycle magnitude that was sometimes smaller than the variations because of inflow turbulence and a significant nonlinear dependence on turbine controller settings.¹⁶ Additionally, a turbine with a sizeable yaw offset angle will experience asymmetric loading on the rotor and drivetrain, and higher yaw moments on the support structure.¹⁷ The direction of yaw offset is also of importance, as blade fatigue in past experimental work have shown opposite trends for flapwise and edgewise components, wherein one increases with positive yaw offset while the other decreases, and vice versa.^{18,19} Partial waking of downstream turbines must also be considered. The unsteady nature of the flow field and imperfect decisions by a farm-level controller could lead to partial waking of the downstream turbine, which is perhaps even more detrimental to fatigue loading than being fully waked.^{19,20} While mean loads tend to follow the power production level and inflow velocity normal to the rotor plane, fatigue loads increase for both the upstream—due to skewed flow—and downstream turbines—due to partial waking.²⁰ Others also observed that yaw offset and partial waking could augment yaw moments on the support structure, but that these added loads could also be shed downstream with counter yaw offsets.^{21,22}

These past studies provide focused insight into loads response due to wake steering; however, there is limited insight into the whole-turbine and whole-array impact of wake steering, motivating a more extensive loads assessment. The publication by Kanev et al²³ is the most similar to our aims here. In that work, a higher-fidelity flow model was used in conjunction with a loads lookup table for a whole-turbine perspective on fatigue loads for a 25-turbine array, each with a rated power of 3.6 MW. Their key finding, consistent with others, is that yaw offsets can increase fatigue loads on the turbine by $\mathcal{O}(10\%)$ due to wind shear on the yawed rotor plane. However, this added fatigue load is counterbalanced by the reduction of wake-added turbulence impinging on the downstream turbines. Thus, when taken over the entire range of the wind rose and operating conditions, the use of wake steering actually reduces lifetime fatigue loading.²³

The objective of this work is to assess the loads impacts of wake steering via yaw offset at the wind-farm scale under a broad set of inflow conditions. This is accomplished using state-of-the-art farm-level modeling to characterize the loads impacts of wake steering via yaw offset on a 12-turbine array of 15-MW fixed-bottom offshore turbines atop monopile substructures. This paper provides two key contributions to the literature with respect to the loads impact of wake steering. The first is the use of the International Energy Agency (IEA) Wind 15-MW reference wind turbine²⁴ as a stand-in for the latest commercially available turbine models. The IEA Wind reference turbine has a significantly higher hub height, larger rotor diameter, and higher thrust and torque values, leading to much stronger wake vortices that persist further downstream compared to prior studies. Second, instead of focusing on a limited number of inflow conditions, load channels, or number of turbines, the intention is to characterize the loads impact from wake steering across the whole turbine and farm for a large range of operational conditions. This includes an examination of mean loads, standard deviations, ultimate loads, and fatigue loads across a 12-turbine array for over 20 quantities of interest (QoI). The work of Kanev et al²³ used an aero-servo-hydro-elastic turbine model for smaller land-based machines. A key difference with our work is that we consider a lower-fidelity farm flow model with an offshore focus using larger turbines.

2 | APPROACH AND METHODOLOGY

This section provides an overview of FAST.Farm, the core model used for flow-field and turbine loads calculations, with an overview of the calibration effort to ensure the model was valid for the application. A description of FLORIS is also provided, as it was the basis for computing the optimal yaw offset angles for wake steering, which only accounted for power production.

2.1 | Overview of FAST.Farm

FAST.Farm is a multiphysics engineering tool that accounts for wake interaction effects on turbine performance and structural loading within wind farms.²⁵ FAST.Farm is an extension of the National Renewable Energy Laboratory (NREL) software OpenFAST,²⁶ which solves the aero-hydro-servo-elasto dynamics of individual turbines. FAST.Farm extends this analysis to include wake deficits, advection, deflection, meandering, and merging for wind farms. FAST.Farm is based on the dynamic wake meandering model,²⁷ with an enhanced implementation to address limitations in prior work. Using this method, the wake deficit of each turbine is computed using the steady-state thin shear layer approximation of the Navier–Stokes equations, and the wake in its downwind propagation is perturbed with a turbulent freestream to capture wake meandering. When skewed flow is present, as in wake steering, the induction is not aligned with the wind direction. In this case, wake deflection is considered by accounting for the induction in the wake propagation. Wake merging is modeled using a superposition method. Each turbine is modeled using OpenFAST, in which the rotor aerodynamics are modeled using the blade-element-momentum theory with options for advanced corrections, including skewed flow, dynamic wake, and unsteady airfoil aerodynamics.

It should be noted that the results presented in this work are derived through simulation, so limitations of the engineering tool may affect the conclusions. Two model limitations relevant to this work are the absence of wake curl under skewed flow and wake-added turbulence. FAST.Farm has been shown to reasonably predict wake deflection in skewed flow,¹⁹ but the physics of skewed-flow-induced counterrotating vortices are not currently modeled, which have an impact on the wake recovery, wake deficit asymmetry, and secondary wake steering. Also, FAST.Farm has been shown to accurately predict turbine power and loads in neutral and unstable atmospheric boundary layer flows with moderate-to-high levels of turbulence,¹⁹ but wake-added turbulence has been shown to be an important driver of fatigue loading for lower turbulence levels.²⁸

FAST.Farm uses several user-specified parameters in the wake dynamics formulation that were specially calibrated for this work. Prior to this study, these parameters had been calibrated for the smaller NREL 5-MW turbine²⁹ using the large-eddy simulation computational fluid dynamics code SOWFA. In this work, a series of similar tuning activities were performed via parameter optimization to better calibrate FAST.Farm against the SOWFA simulations for the IEA Wind 15-MW reference wind turbine with stronger thrust and wake vorticity. The chosen test cases consisted of three turbines aligned to the inflow, spaced seven rotor diameters apart. Time-series and probability density functions for rotor power, rotor torque, rotor speed, and wake deflection were compared (FAST.Farm versus SOWFA) for a set of six combinations of TI and yaw angle. For all cases with turbine yaw offset, there were some differences for all QoI and all turbines, including front-row turbines. This was unexpected based on past comparisons with smaller turbines^{19,30} and likely due to improper tuning of the FAST.Farm parameters that adjust the horizontal wake deflection. The parameter values were tuned using a grid search and optimization focusing on minimizing the error between FAST.Farm and SOWFA in the wake deflection and power generation of the two downstream turbines. A full description of these parameters and the tuning process is fully described in Appendix A. The remaining differences were deemed acceptable for the subsequent analysis.

2.2 | Modeling cases and setup

To capture a full range of operational conditions, a wide range of parametric inflow conditions and turbine alignments were used, described in Table 1. The parameterization is meant to represent the normal operational design load cases 1.1 and 1.2 for ultimate and fatigue loads, respectively, in the International Electrotechnical Commission (IEC) 61400-series standards for wind turbine design.³¹ A few modifications were made to the IEC specifications to represent variations that are important for assessing the load impacts from wake steering. These modifications were:

TABLE 1 Parametric inflow property variation for FAST.Farm simulation

Parameter	Values
Hub-height velocity [m/s]	6.6, 8.6, 10.6, 12.6, 16.6
Shear exponent [-]	0.1, 0.2, 0.3
Turbulence intensity [-]	Class B, C, D
Inflow wind direction [deg]	−20 to 20 in steps of 2

- Adding a lower turbulence class, where wake steering is more applicable, referred to as Class D ($I_{Ref} = 0.10$);
- Sweeping a range of power-law shear exponents;
- Sweeping of inflow wind directions;
- Using only the expected value of significant wave height and peak-spectral wave period at each mean wind speed because the hydrodynamic loads are not expected to affect quantities of interest other than loads at the mudline;
- Neglecting loads extrapolation in design load case 1.1; and
- Comparing non-yawed and wake steering load profiles.

The selected wind speeds are derived as offsets from the rated speed of 10.6 m/s. The associated turbulence intensity percentages based on turbulence class are shown in Figure 1. In total, there were 45 inflow conditions and 21 inflow directions, with 0° indicating flow straight down the rows from the left to right in Figure 2.

Ambient wind inflow is synthetically generated with TurbSim,³² which creates time-varying two-dimensional inflow turbulent flow fields using the Kaimal turbulence spectrum with an exponential coherence model following standard IEC turbulence conventions. Within FAST.Farm, these turbulent flow fields are propagated along the wind direction at the mean wind speed of the midpoint of the field. Six different random turbulence seeds were used to generate the inflow data for each inflow condition, and six corresponding seeds were used for the irregular waves. This was done to capture variability in the numerical simulation results due to the stochastic nature of turbulence and waves. Each FAST.Farm simulation for every inflow condition and angle was repeated for each of the six random seeds. Inflow wind direction variations were modeled in FAST.Farm by repositioning the wind turbines in the domain rather than by actually changing the wind direction. In total, this parameter space required 270 TurbSim simulations and 11,340 FAST.Farm simulations.

Wave data for the offshore wind farm was taken from buoy measurement data along the U.S. East Coast. The measurement data were processed to determine the significant wave height and peak-spectral wave period of the offshore environment. The significant wave height represents the expected value of the wave height conditioned on each mean wind speed. The peak wave period represents the average peak wave period conditioned on mean wind speed and significant wave height. The incident waves propagated in a direction aligned with the wind. The resulting values used in the FAST.Farm simulations are summarized in Table 2. These conditions are well below breaking wave conditions.

The IEA Wind 15-MW reference wind turbine is used for all simulations. This turbine has a hub height of 150 m, a rotor radius of 120 m, and a variable speed, collective pitch controller with different modes of operation at below-rated and above-rated wind speeds. The performance curves for the reference turbine, which can be helpful in interpreting the load trends in this work, are found in Figure 3. Structural dynamics of the blades, drivetrain, tower, and substructure; hydrodynamic wave loading on the monopile; and the response of the wind turbine control system, including variable-speed torque control and collective blade-pitch control, are also modeled in OpenFAST. FAST.Farm simulations were performed with a high-resolution inflow box around each turbine and a lower-resolution box elsewhere in the domain. The higher-resolution spatial discretization was 5 m, which is fine enough to excite the turbine response considered in this paper. The temporal discretization was 0.5 s to capture the high-frequency content in the turbine loads past six per revolution (6P). Low-resolution spatial and temporal discretization vary between cases

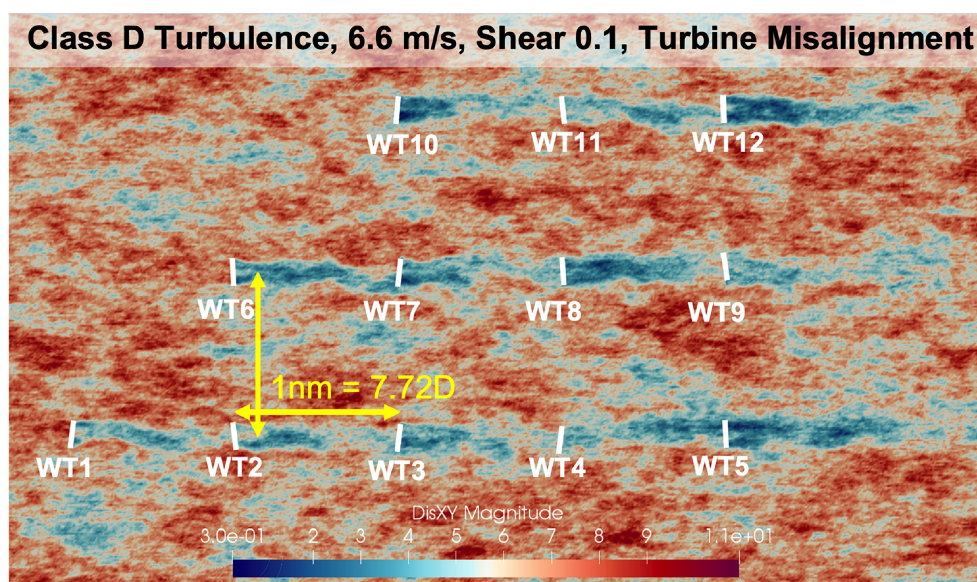


FIGURE 1 Instantaneous two-dimensional flow visualization of a 12-turbine FAST.Farm simulation with 7.72 rotor diameter streamwise and transverse turbine spacing, 6.6 m/s inflow velocity, Class D turbulence, and a shear exponent of 0.1, colored by velocity magnitude

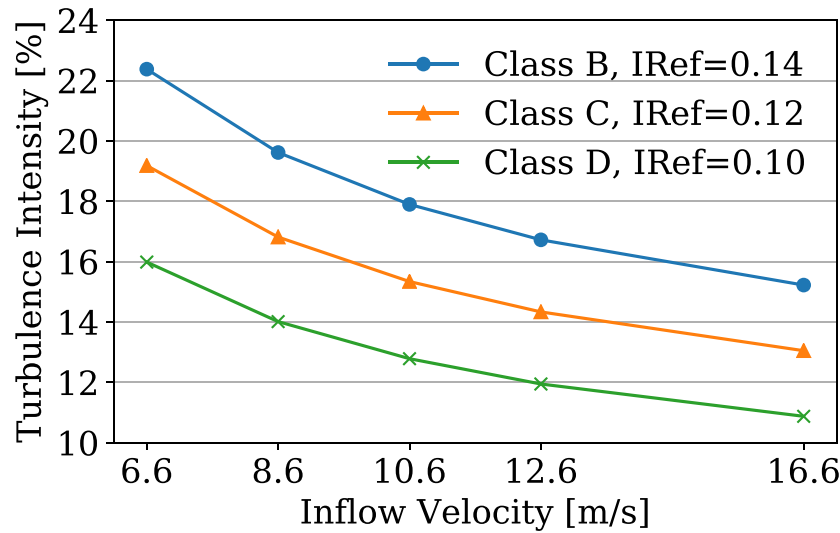


FIGURE 2 Turbulence intensity (TI) percentage based on TI class and mean hub-height inflow velocity

TABLE 2 Significant wave height and peak-spectral wave period based on average hub-height inflow velocity

Inflow velocity (m/s)	Sig. wave Height [m]	Peak wave period [s]
6.6	1.172	7.287
8.6	1.323	6.963
10.6	1.523	7.115
12.6	1.764	6.959
16.6	2.255	7.067

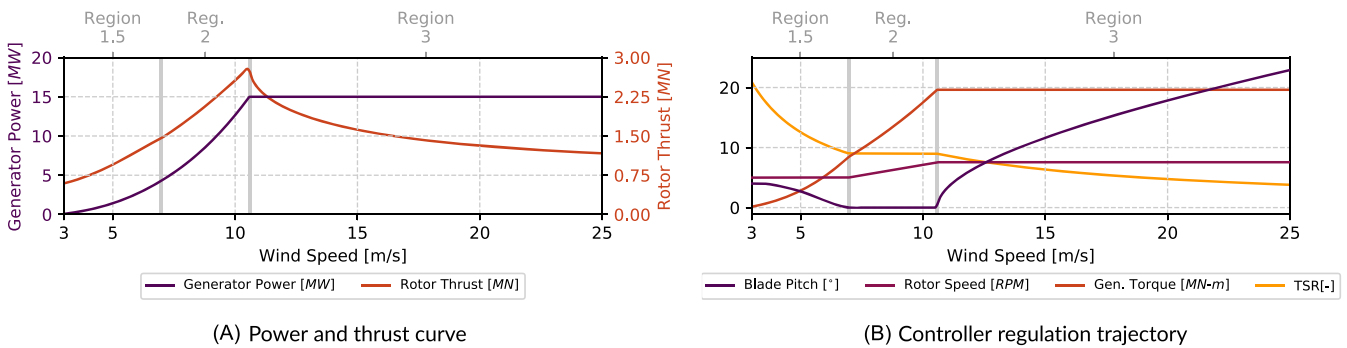


FIGURE 3 OpenFAST blade element momentum performance and operation of the IEA Wind 15-MW reference wind turbine rotor with the ROSCO controller²⁴

based on average hub-height inflow velocity, following the guidance derived from Shaler et al.³³ Total simulated time for each simulation was 2,000 s including 300 s for initial transients, not included in the analysis.

2.3 | FLORIS optimization

FLORIS is an open-source model designed to provide a computationally inexpensive, controls-oriented representation of the steady-state wake characteristics in a wind farm.³⁴ This makes it well suited to optimization of yaw offsets for wake steering and/or array layout to minimize wake losses. For each inflow case, a standard array was simulated without mean yaw offsets and compared against simulations with wake steering via yaw offsets. The yaw offsets of each turbine were calculated for each inflow case and inflow angle using an offline optimization with FLORIS.

Yaw optimization results were independent of TI class. Note that the yaw optimizations were performed for a larger wind farm, of which the 12-turbine array is a subset of the most upstream turbines with 7.72 rotor diameter streamwise turbine spacing in the corner of the wind farm. Additionally, within FLORIS the yaw offsets were selected for maximizing the total wind farm power output for each inflow case and inflow angle and no consideration was given to minimizing turbine loads.

The optimized yaw offsets are shown in Figure 5, using a single pixel for each inflow case as shown in Figure 4. A few immediate observations are worth noting. First, there is no wake steering above rated conditions (Region III of the power curve) or for inflow angles above $\pm 10^\circ$. Second, positive and negative yaw offset angles were used for all turbines. The use of negative yaw offset angles is an active area of exploration with open questions as to whether FLORIS has sufficient fidelity to capture the necessary physical nuances in this flow regime. Likely, the optimizer is observing that in FLORIS, deflecting the wake the opposite direction lowers the aggregation of wakes downstream. Although similar yaw offset angles were used for all turbines, there were some differences between turbines, particularly for WT1. For WT1, the front turbine for the 5-turbine row at the bottom of the wind farm, the use of negative yaw angles may extend even to the zero-degree inflow case, whereas for all other turbines, negative yaw angles are associated with negative inflow angles. In this work, which is focused more on loads analysis, the use of negative yaw angles does impact the loading trends and might also play a role in augmenting or diminishing the negative effects of partial waking for inflow directions that are misaligned with the turbine array.

2.4 | Quantities of interest

One of the differentiating features of this work is consideration of full wind turbine and farm loads. Thus, the results are broken down by QoI, which encompass turbine operational parameters, such as rotor speed or blade pitch, and key structural loads or deflections, such as tower-base moment or out-of-plane blade-tip deflection. The full list of QoI in the analysis is shown in Table 3, some of which are further broken down into vector components. Time-domain histories of the QoI are presented via aggregate statistics including mean values, standard deviations, ultimate loads, and short-term damage equivalent loads (DELs). For conciseness, not all QoI are presented for all inflow conditions, angles, and summary statistics. Additionally, for some QoI, the mean value may be zero. Given the comparison of turbines without yaw offset versus with yaw offset, the coordinate system definition of fore-aft or side-side can be different. Therefore, only a vector magnitude is considered in the mean and ultimate results for the QoI with those vector components. For postprocessing of fatigue results, see the discussion in the next section.

2.4.1 | Statistical calculations

A cross section of the results is presented in two stages. First, the mean value and standard deviation statistics are presented for a subset of the conditions to serve as building blocks for understanding the underlying dynamics. Next, ultimate and fatigue loads are analyzed for all conditions; these quantities directly address the central question of whether wake steering with yaw offsets is deleterious to the turbine load envelope.

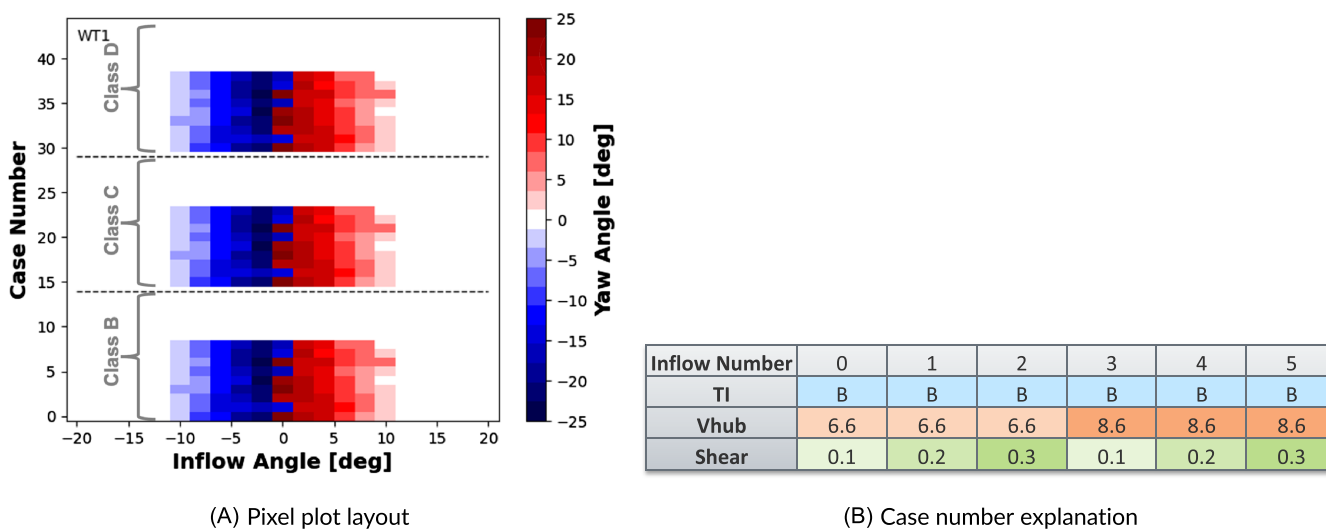


FIGURE 4 Explanation of pixel plots depicting yaw offset values for all inflow conditions and directions. In the pixel plots (A), the x-axis specifies the inflow angle and the y-axis specifies the inflow condition looping over TI, then velocity, and then shear. A sample of the inflow condition looping is provided in (B)

TABLE 3 Quantities of interest and associated applicable vector components used in the analysis

Quantity of Interest	Component		
Generator power			
Rotor speed			
Rotor torque			
Rotor thrust			
Blade pitch			
Blade-tip displacements	Out-of-plane	In-plane	
Blade-tip tower clearance			
Blade-root moments	Out-of-plane bending	In-plane bending	Pitching
Low-speed shaft moment at main bearing	0° bending	90° bending	
Tower-top deflections	Fore-aft	Side-side	
Tower-top moments	Fore-aft bending	Side-side bending	Yaw
Tower-base moment	Fore-aft bending	Side-side bending	Yaw
Mudline moments	Fore-aft bending	Side-side bending	Yaw

Mean time-averaged and standard deviation statistics were calculated using standard methods for each time history and then averaged across all seeds. Ultimate loads were computed by averaging the sum of the maximum values from each seed, where S is the total number of seeds (six).

$$Ult = \frac{1}{S} \sum_{s=1}^S \max|x_s|. \quad (1)$$

Both short-term and pseudo-lifetime fatigue DELs are presented in this work. Short-term DELs of a given QoI were computed directly from the time series as an aggregate across all seeds using the NREL postprocessing tool, MLife.³⁵ Rainflow counting was used to bin a histogram of load cycle amplitudes over the time series. In this case, no Goodman or other mean-value correction was applied to the histogram amplitudes. The short-term DELs were computed from the histogram bins and the material-specific Wöhler exponent, m , from classical S-N fatigue theory, as in Equation (2). As is standard practice, $m = 4$ was used for loads on steel components (main shaft, tower, and monopile), and $m = 10$ was used for blade loads as a composite material.

$$DEL_{short} = \left[\frac{1}{T} \sum_k n_k f_k^m \right]^{1/m}. \quad (2)$$

Here, T is the simulation time representing a 1-Hz equivalent cycle, k is the number of bins, and n is the number of cycles at load amplitude, f . For fatigue of vector-component QoI, such as blade-root, tower, and monopile bending moments, a load rose analysis was applied with a 10° increment, from which the maximum DEL around the rose was selected.

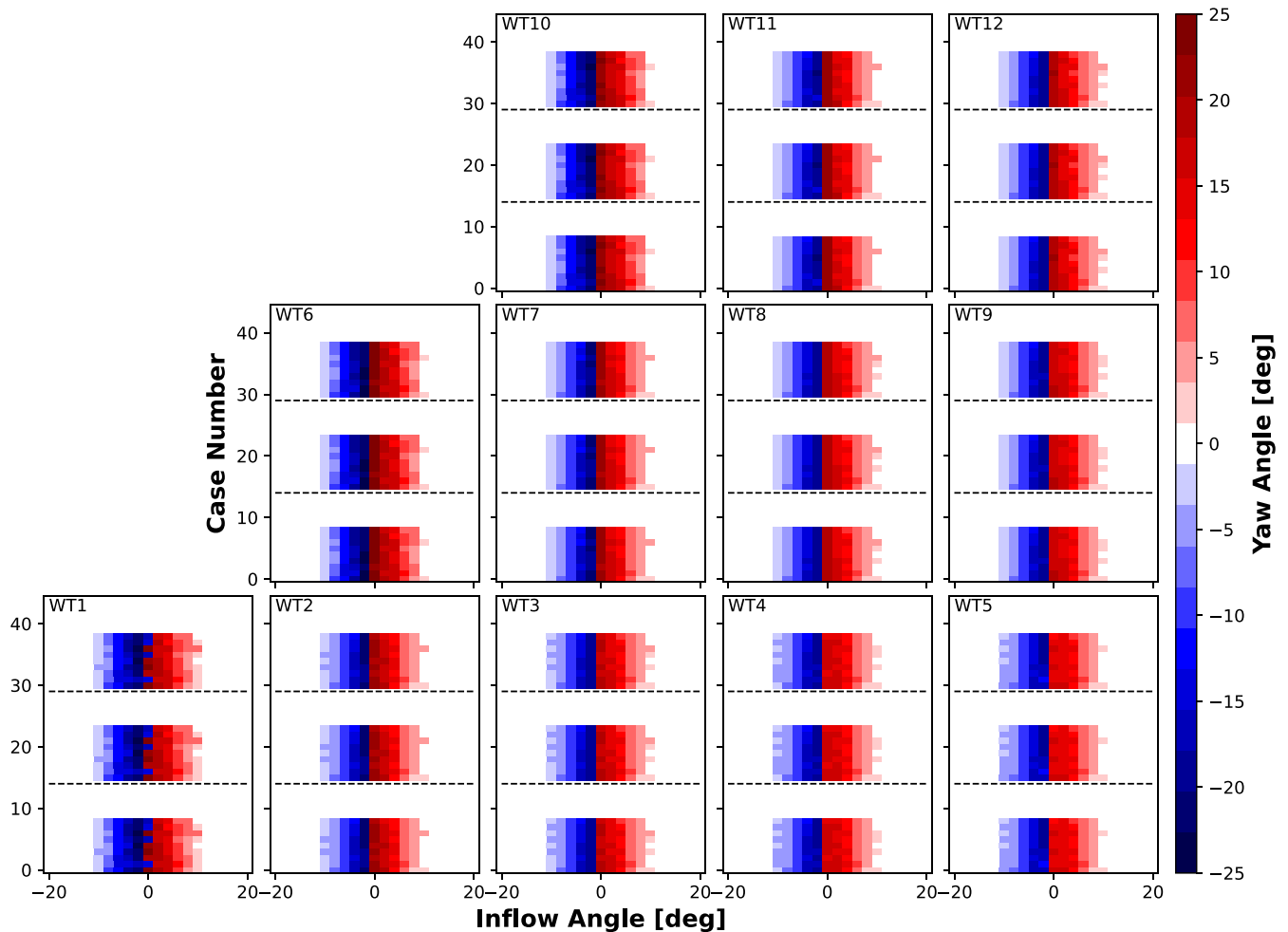
To combine multiple short-term DELs into a pseudo-lifetime measure, the frequency or probability of a given inflow condition is needed to weight the short-term value. Wind speed variation used normalized probabilities from extrapolations of buoy measurements. All other inflow conditions were considered equally because there was no site-specific joint probability distribution of inflow conditions to assign probabilities. More specific probabilities could be specified for these quantities with available measurement data. Pseudo-lifetime DELs are then computed as

$$DEL_{life} = \left[\sum_i^N \sum_j^{N_{vel}} \phi_i \phi_j DEL_{short,ij}^m \right]^{1/m}, \quad (3)$$

where ϕ_i is 1 divided by the number of inflow cases considered, N (not counting velocity), and ϕ_j is the normalized probability for each velocity. Table 4 lists the ϕ_j values for each velocity bin. In Section 3.2.3, pseudo-lifetime DELs are examined for both the full set of all inflow cases and also the smaller subset, in which only wake steering is used in Figure 5. Therefore, ϕ_j takes on different values for each set of cases.

TABLE 4 Scaled probability of a particular wind speed for all cases and wake-steering-only cases

Inflow velocity (m/s)	6.6	8.6	10.6	12.6	16.6
All cases	0.230	0.242	0.269	0.201	0.057
Wake steering only	0.311	0.327	0.362	0.0	0.0

**FIGURE 5** Optimized yaw offset angles for wake steering for all turbines in array. Subfigures are arranged to be the same as the wind farm turbine layout

3 | RESULTS

The key findings in this paper are communicated in a series of event tables and plots at the end of this section, focusing on ultimate and fatigue loading due to the use of wake steering. These quantities directly address the central question of whether wake steering with yaw offsets is deleterious or beneficial to the turbine load envelope. However, it is easier to understand these aggregate results by first visiting simpler comparisons where load channel behavior through the array is compared across parametric changes in inflow conditions for simple statistics such as mean values or standard deviations of the time series. These sensitivity studies serve as building blocks to the key findings and are presented first using mean value and standard deviation statistics.

3.1 | Mean values and standard deviations

Time-series statistics for the zero-degree inflow direction and varying inflow directions are shown in Sections 3.1.1 and 3.1.2, respectively. For all of the figures presented in this subsection, the non-yawed turbine simulations (no wake steering) are in the left-hand column and the yaw-

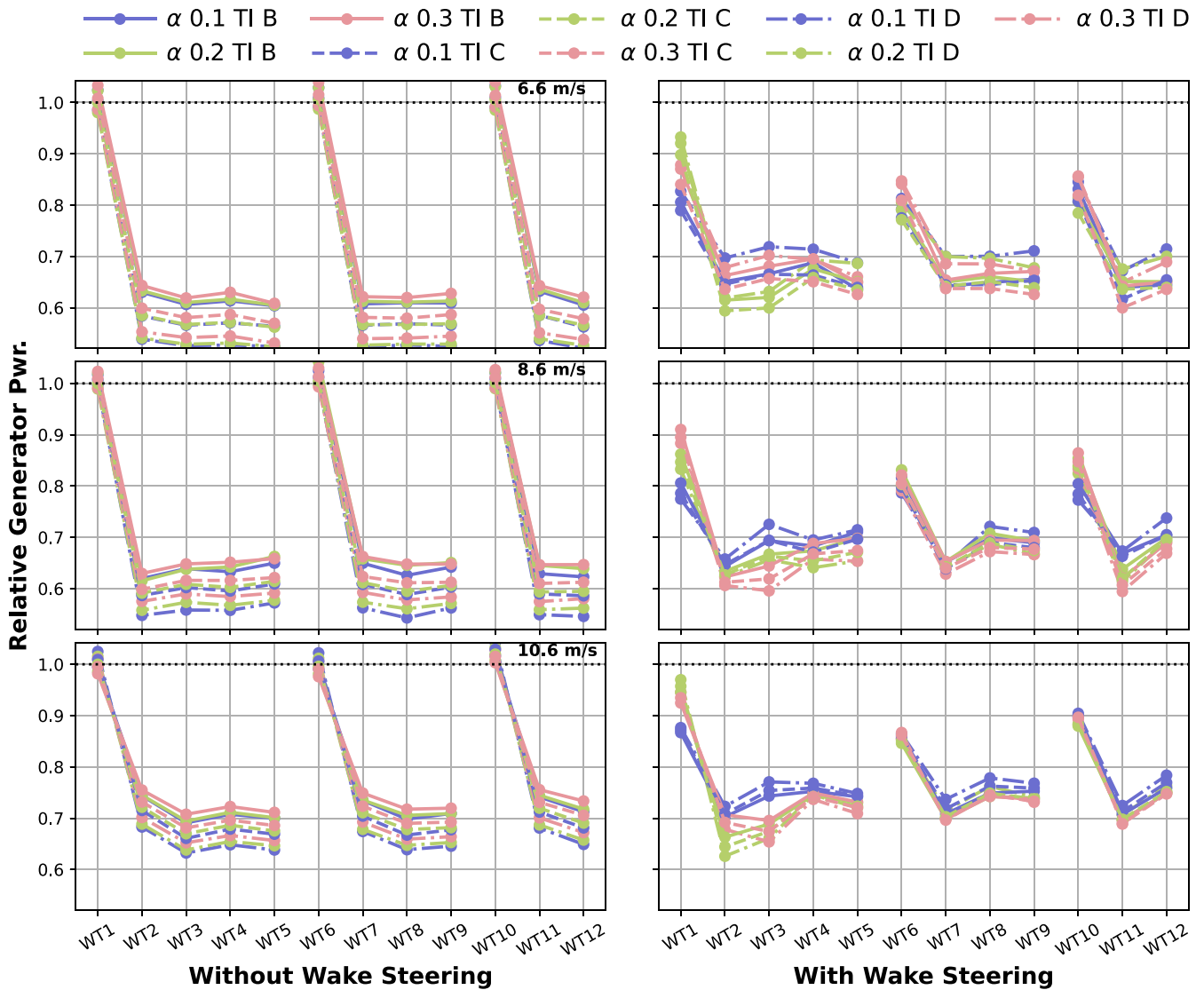


FIGURE 6 Time-averaged results for each turbine relative to WT1 without wake steering. Each subplot shows results without wake steering (left) and with wake steering (right). Each row corresponds to a different inflow velocity. Turbine rows are denoted with vertical lines

optimized turbines using wake steering are in the right-hand column. Each row corresponds to a wind speed bin, from 6.6 to 10.6 m/s, with comparisons at higher velocities excluded because there is no wake steering above rated conditions. All 12 turbines are arranged on the x-axis. All results in Figures 6–10 are normalized by the QoI statistic value of the first turbine (WT1) at the central inflow condition of TI Class C, shear exponent of 0.2 (green dashed line), zero-degree inflow, and zero-degree yaw offset (no wake steering).

3.1.1 | Zero-degree inflow angle, varying inflow conditions

Results in this section vary the shear-TI inflow condition while keeping the inflow angle fixed at zero degrees (aligned with the array). Each line represents a different inflow condition with shear power law exponent (α) designated by line color and TI designated by line style.

Figure 6 shows the mean value for generator power at a zero-degree inflow angle (aligned with the array), with varying shear and TI inflow conditions. For the non-yawed results (left-hand side), all downstream turbines have a significant and consistent drop in power production, with some stratification according to TI and shear. For the yawed results (right-hand side), there is some drop in power production for the front-row turbines, but a smaller decrease for downstream turbines, leading to a more even power production level throughout the array. Generally, higher TI results in more power for the downstream turbines due to faster wake recovery. This same behavior is seen for rotor thrust, torque, out-of-plane blade tip deflection, blade-root out-of-plane bending moment (Figure 7A), tower-base fore-aft bending moment (Figure 7C), and mudline (monopile base) bending moment, although not all of these QoI are shown.

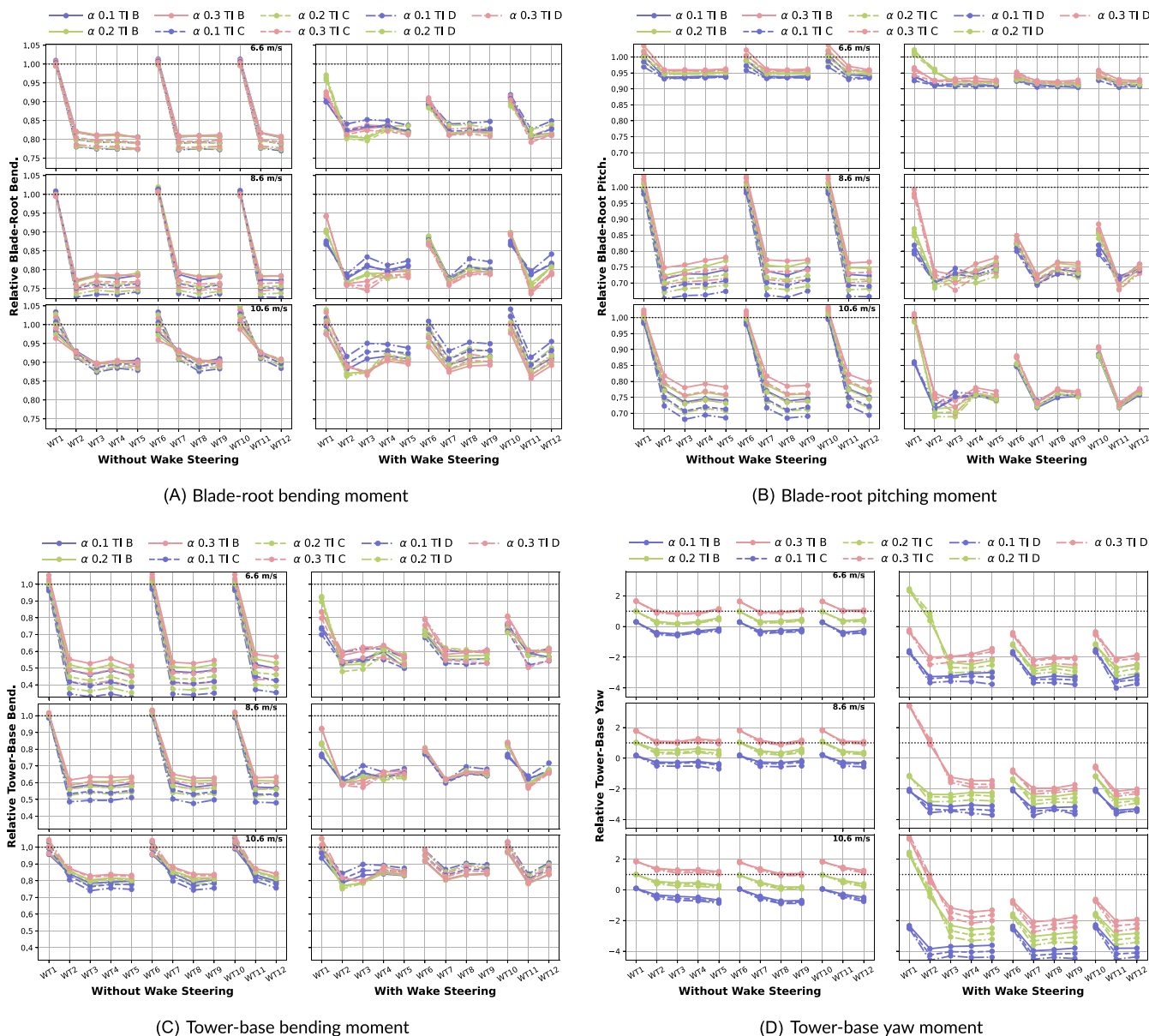


FIGURE 7 Time-averaged results for each turbine relative to WT1 without wake steering. Each subplot shows results without wake steering (left) and with wake steering (right). Each row corresponds to a different inflow velocity. Line color corresponds to shear exponent value; line style corresponds to TI class

Figure 7 shows the mean value for several QoI at a zero-degree inflow angle (aligned with the array), with varying shear and TI inflow conditions. Figure 7A,C follows the same trends as generator power. Similar observations are made about blade-root pitching moment, shown in Figure 7B. The non-yawed results show that all downstream turbines have a significant and consistent drop in blade-root pitching moment, with some stratification according to TI and shear. This stratification is present for both front-row and downstream turbines. There is less variation in downstream turbine results at the lowest wind speed due to rotor operation at the fixed minimum rotational speed. For the yawed results, there is some drop in pitching moment for the front-row turbines compared to the non-yawed results, but a smaller decrease for downstream turbines, leading to more even values throughout the array. This same behavior is seen for rotor speed, although it is not shown here. The inconsistent results for WT1 at a couple of the inflows are due to the use of negative yaw angles.

Different observations are made about tower-base yaw moment, shown in Figure 7D. For the non-yawed results, there is a strong grouping of results by shear because yaw moments are a reflection of force imbalances on the rotor; these imbalances increase with shear value. There are also minimal reductions in yaw moment for downstream turbines. For the yawed results, there is a slightly higher degree of variation between

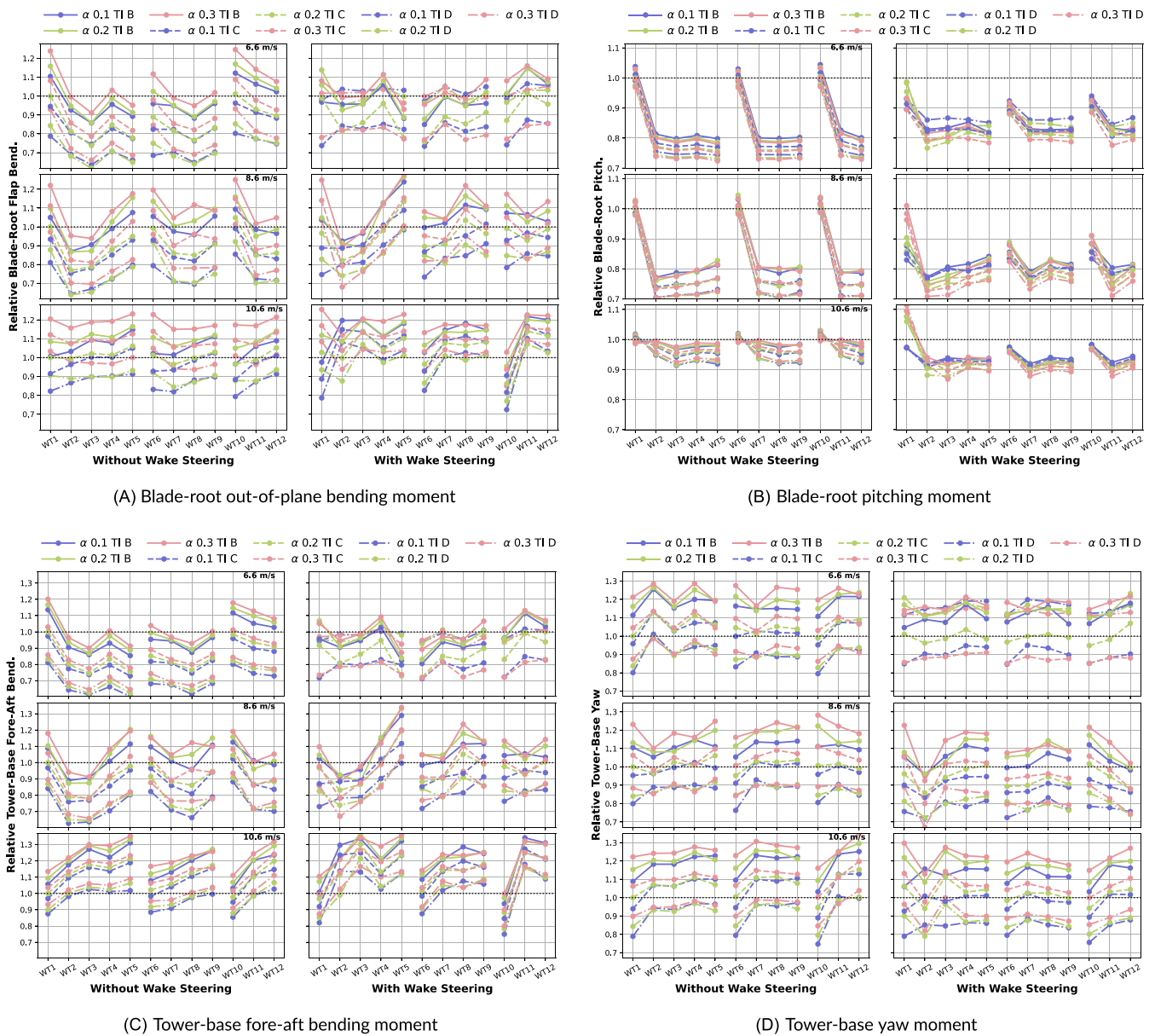


FIGURE 8 Standard deviations of time series for each turbine relative to WT1 without wake steering. Each subplot shows results without wake steering (left) and with wake steering (right). Each row corresponds to a different inflow velocity. Line color corresponds to shear exponent value; line style corresponds to TI class

upstream and downstream turbines. Note that WT1 stands out as an outlier due to the occasional use of negative yaw angles. However, the overall yaw moment value is less than the non-yawed results, contrary to expectations that the yaw offsets would create significant yaw moments on the support structure. This same behavior is seen for tower-top and mudline yaw moments.

The results in Figure 7 show that without wake steering, whether or not a turbine is within the wake of an upstream turbine is a stronger driver of the mean loads than variations in TI or shear value. With wake steering, there is more even mean loading along the array rows, and at a lower magnitude. This could imply an operational benefit of more uniform loading and operational wear across all turbines. Finally, the negative yaw angle for WT1 causes some nonintuitive loading behavior and is worth further investigation.

Shown in Figure 8 are time-series standard deviation results for several QoI at a zero-degree inflow angle (aligned with the array), with varying shear and TI inflow conditions. As with the mean results, some yawed results for WT1 are outliers due to the use of negative yaw angles. For all non-yawed results, standard deviations are grouped by TI as the primary trends driver because higher TI leads to higher standard deviation of the inflow wind. For blade-root out-of-plane and tower-base fore-aft bending moments, shown in Figure 8A,B, the non-yawed standard deviation results dip slightly for the first few downstream turbines at lower velocities, but increase slightly for the more

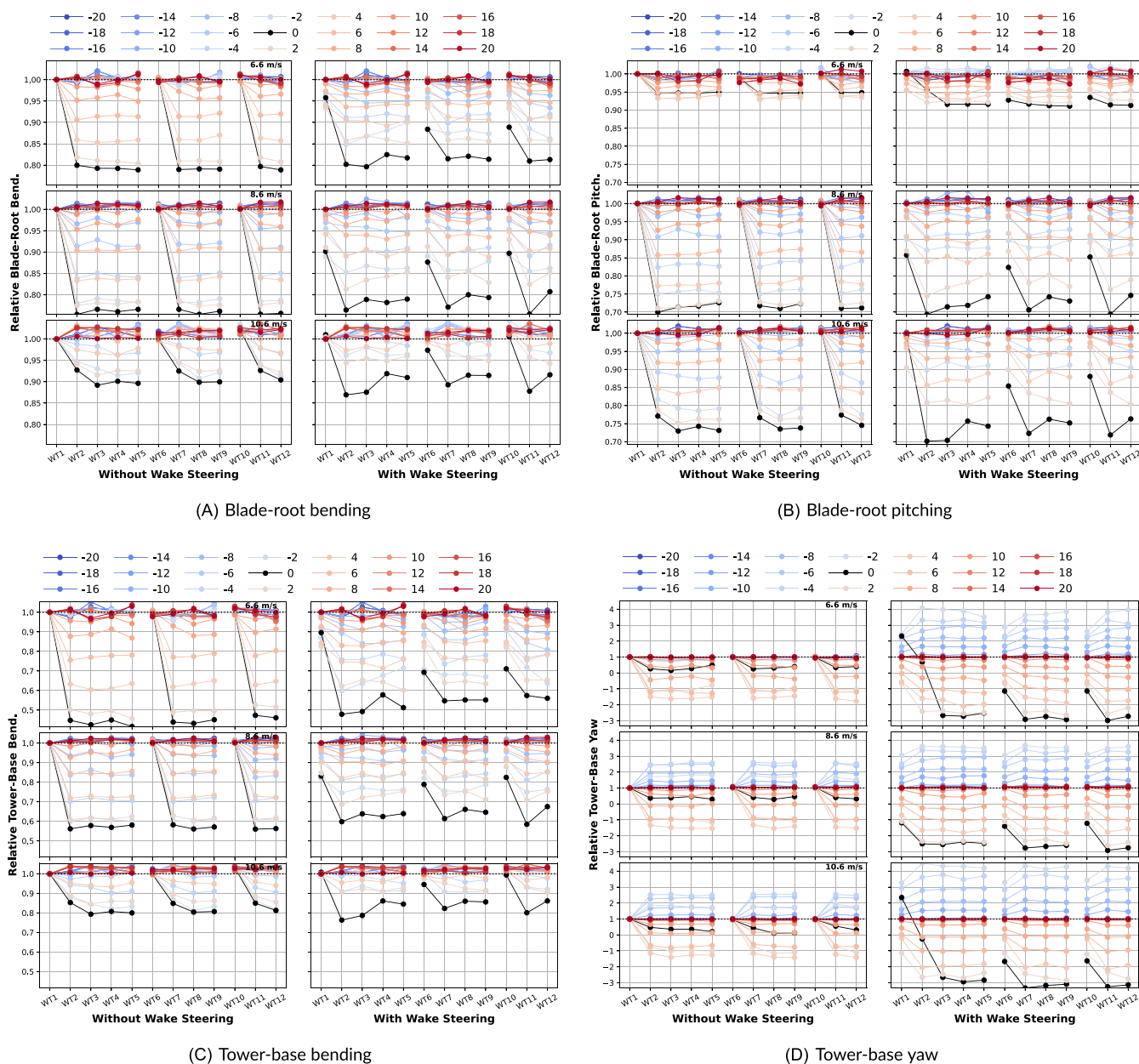


FIGURE 9 Time-averaged results for each turbine relative to WT1 without wake steering. Each subplot shows results without wake steering (left) and with wake steering (right). Each row corresponds to a different inflow velocity

downwind turbines and at rated speed. These results are from a combination of the buildup of wake-meandering-induced turbulence down the row and because the highest sensitivities and largest variations in turbine response are at rated conditions. Additionally, for tower-base fore-aft bending and yaw moments, there is not a pronounced difference for the yawed results, suggesting that wake steering does not have a pronounced effect on fatigue cycle for those loads. This same behavior is seen for rotor torque, rotor thrust, tower-top fore-aft displacement, and mudline fore-aft moment. Blade-root pitching moment results, shown in Figure 8A, have the same grouping by TI, but also a more noticeable decrease in standard deviations for non-yawed, downstream turbines at below-rated inflow velocities. At rated inflow velocities, the blade-root pitching moment is more constant. For yawed results, there are smaller differences between front-row and downstream turbines for a more uniform loading. Tower-base yaw moment results, shown in Figure 8D, display the same grouping by TI and also that the downwind turbines experience an elevated level of tower-base yaw moment standard deviation, likely due to the impact of wake meandering causing partial waking of the downwind rotors. Similar trends are seen for tower-top and mudline yaw moments.

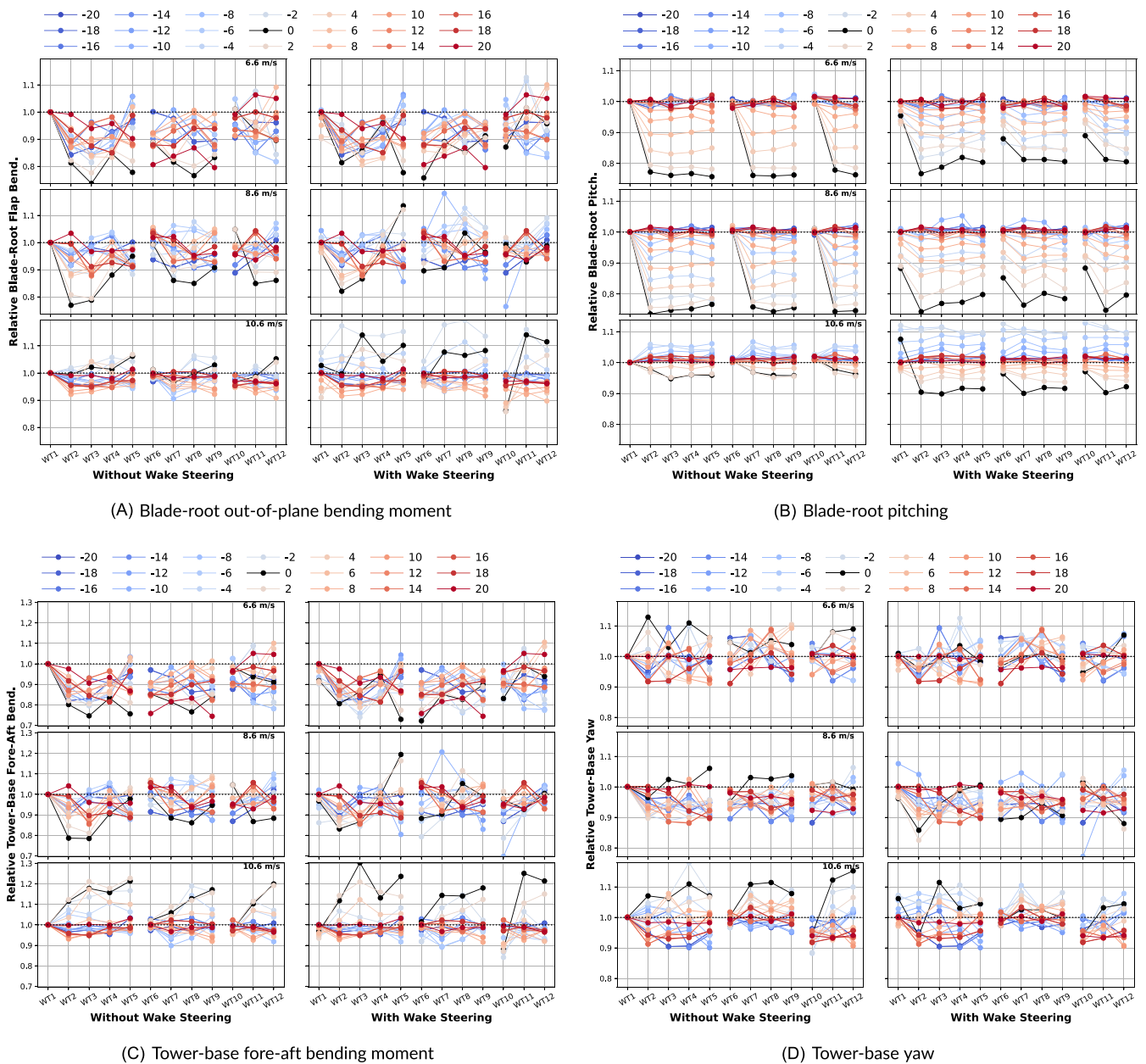


FIGURE 10 Standard deviation of results for each turbine relative to WT1 without wake steering. Each subplot shows results without wake steering (left) and with wake steering (right). Each row corresponds to a different inflow velocity

3.1.2 | Varying inflow direction, single inflow condition

This section presents the same QoI statistics, but shear and TI are held fixed at the central values ($\alpha=0.2$, TI class C). Instead, the inflow angle is varied from -20° to $+20^\circ$ relative to the array orientation. For each inflow angle, the mean yaw error for each wind turbine is zero for the non-yawed results and offset from zero for the cases with wake steering. Each line represents a different inflow angle, with the darker the red, the more positive the inflow angle and the darker the blue, the more negative the inflow angle. A black line is used for the zero-degree inflow case and shows the same result as the green dashed line in Figures 7 and 8.

Figure 9 shows the mean value for several QoI across varying inflow angles. For tower-base bending and blade-root bending and pitching moments, shown in Figure 9A–C, both non-yawed and yawed results show that there is a gradual increase in the mean structural loading of downstream turbines with increasing absolute inflow angle as wake effects diminish and each turbine eventually becomes a “front-row” turbine. There are also small differences between positive or negative inflow angles. With wake steering, there is reduced mean loading for front-row

turbines, but increased mean loading for downstream turbines, resulting in more even load distribution across the wind farm. All cases with positive inflow angles have positive yaw angles, while all cases with negative inflow angles have negative yaw angles, respectively. The turbines in the zero-degree inflow case (black line) have positive yaw angles, except for WT1; therefore, the result of WT1 is more in line with the positive inflow cases. Similar trends are seen for generator power, rotor thrust, rotor torque, blade tip in-plane and out-of-plane deflections, and mudline bending moments.

Tower-base yaw moment results in Figure 9D show much different trends. As expected, the normalized mean moments approach unity for inflow angles above $\pm 10^\circ$. However, for the non-yawed results with positive inflow angles under 10° , downstream turbine mean moments are below the zero-degree inflow results. Additionally, for negative inflow angles above -10° , the downstream turbine mean moments are higher than the zero-degree inflow results. This could be due to partial waking and whether the wake impinges more on the rising or falling blade, given the clockwise rotor rotation.³⁶ For the yawed results, the same trends as the non-yawed are observed, but with larger absolute values due to the additional yaw moments from wake steering yaw offset. Additional yaw moments due to wake steering at the zero-degree inflow angle were not observed in Figure 7D, which is represented by the black line in Figure 9. This same behavior is seen for tower-top and mudline yaw moments.

Figure 10 shows the standard deviation for several QoI across varying inflow angles, using the central shear and T1 inflow conditions. Figure 10A shows noisy trends in blade-root out-of-plane bending for both the without and with wake steering simulations. In this case, the load standard deviations are primarily driven by spatial variability in the turbulent flow field, especially at the two lower velocities (explained in greater detail in Appendix B). This spatial variability is due to each wind turbine ingesting different parts of the flow fields as the absolute inflow angle increases. This response is also seen for tower-base fore-aft bending and yaw moments (Figure 10C,D), mudline fore-aft bending and yaw moments, and tower-top fore-aft displacement. Essentially, the standard deviation of the wind field over time can vary spatially even though the turbulence class is the same. This is partly a product of TurbSim generating turbulent flow fields with the specified spatial coherence and Gaussian statistics, which means the standard deviation target value is satisfied in aggregate, but not at every point in the field. This spatial variability of turbulence does lead to some random inconsistencies in inflow conditions between turbines in the FAST.Farm simulation, which can be seen in some load channels that are not otherwise dominated by turbine operations, especially at nonzero inflow angle results. It is likely that using more random turbulence seeds would lead to converged results with more clear trends.

Blade-root pitching moments, shown in Figure 10B, have different trends. For the non-yawed results, the standard deviations decrease for the downstream turbines, relative to the front-row turbines, at the lower velocities. There is more consistent loading at rated conditions, with some positive/negative inflow angle asymmetry. Overall, the normalized results tend towards one as inflow angle increases. For the yawed results, the trends are similar with noticeably less variability across the arrays, but also some exaggeration of the positive/negative inflow angle asymmetry at rated velocity. Once again, the differences in trends for WT1 are due to its use of a negative yaw angle.

3.2 | Ultimate and fatigue loads

Fatigue and ultimate loads across all conditions are analyzed in several ways. First, pixel plots, using the same convention as in Figure 5, are constructed for relative changes for each QoI for the i th turbine at the j th inflow case, using Equation (4).

$$\Delta QoI_{ij} = \frac{QoI_{\text{steering};ij} - QoI_{\text{noSteering};ij}}{QoI_{\text{noSteering};ij}} \quad (4)$$

While these pixel plots identify the impact of wake steering for every QoI and inflow case, they do not compare one case to another and cannot provide an aggregate impact. Therefore, extreme event tables are constructed for ultimate loads, which involves identifying the maximum absolute ultimate load value for each QoI across all inflow cases. This is done separately for the cases with wake steering versus without wake steering via yaw offset. For fatigue loads, a pseudo-lifetime analysis is performed, described in Section 2, and calculated separately for the cases with and without wake steering via yaw offset. Finally, the resulting extreme events values and pseudo-lifetime fatigue loads are plotted across the array to more readily identify farm-level trends.

3.2.1 | Ultimate loads: All cases

Figure 11 shows relative difference pixel plots for each turbine constructed using Equation (4) at each inflow condition and angle combination for ultimate loads. Zoomed-in pixel plots for WT1 and WT2 are shown in Figure 12. Note that a white cell indicates no change with wake steering, a red cell indicates a higher value with wake steering, and a blue cell indicates a lower value with wake steering. For blade-

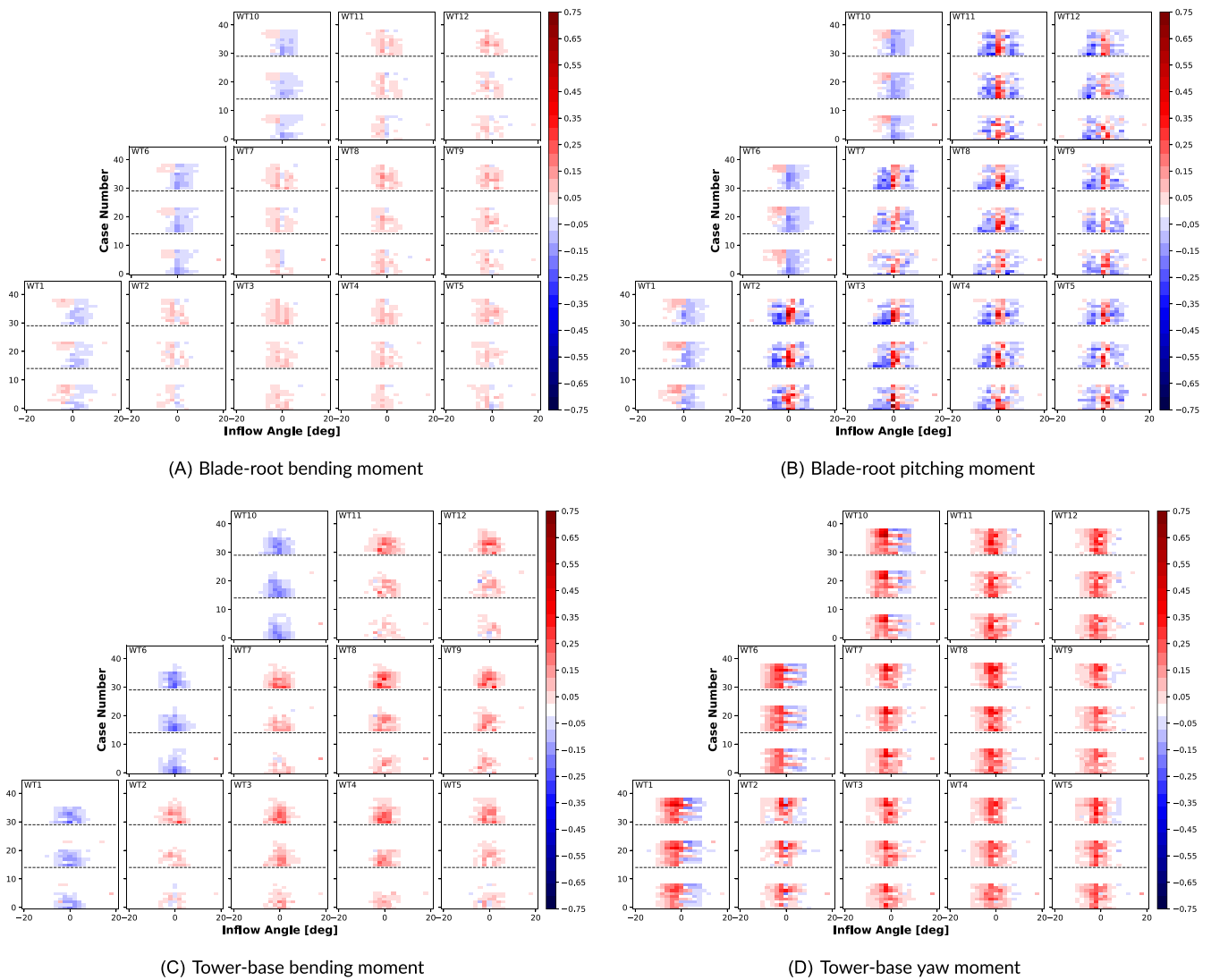


FIGURE 11 Pixel plots of relative difference between ultimate loads for each turbine. Each cell corresponds to a different inflow condition and inflow angle combination. White cells indicate no change with wake steering via yaw offset, red cells indicate a higher value with wake steering, and blue cells indicate a lower value with wake steering

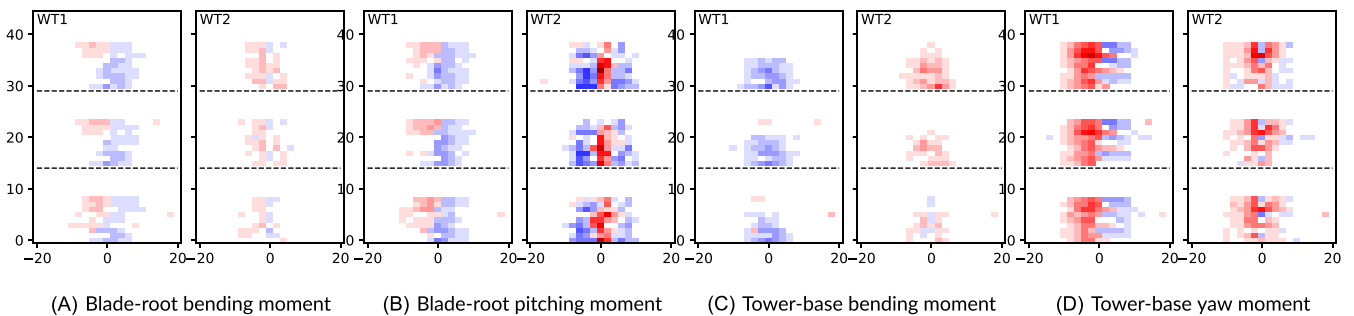


FIGURE 12 Zoomed-in pixel plots of relative difference between ultimate loads for WT1 and WT2. Each cell corresponds to a different inflow condition and inflow angle combination. White cells indicate no change with wake steering via yaw offset, red cells indicate a higher value with wake steering, and blue cells indicate a lower value with wake steering

root total bending moments, shown in Figure 11A, there are mostly white pixels, even more so than in Figure 5, and the red and blue shades are quite light. This conveys that while there are blade-root bending moment differences introduced by wake steering, they are generally small and restricted to select conditions. For downstream turbines, the color shading is red, meaning wake steering increases blade-root

bending, which is consistent with an increase in power production and thrust loads for those turbines. For front-row turbines, the shading is mostly blue, due to reduced power production and thrust loading. However, there is also some red-blue asymmetry at positive versus negative inflow angles and the zero-degree inflow case; this phenomenon is not yet fully understood, but is likely related to the advancing and retreating of the blade operating in a skewed flow. The same trend is observable to an even greater degree for the front-row turbines in the blade-root pitching moment results in Figure 11B. For downstream turbines, the blade-root pitching moment results are much more complex with inflow angles aligned with the array leading to an increase in maximum moment with wake steering, but steeper inflow angles (positive or negative) lead to an ultimate load reduction with wake steering. This is likely due to wake steering at low inflow angles not modifying the wake path enough to fully unwake the downstream turbines at all time steps, with the partial waking increasing blade pitch moments. At steeper inflow angles, the wake steering is enough to fully unwake the downstream turbines at all time steps. This phenomenon is only seen in blade pitching moments because this load is significantly more sensitive to subtle changes in rotor-plane variations and controller behavior.

In contrast to the complexity for blade-root pitching moment, the tower-base total bending moment results in Figure 11C are more intuitive. Wake steering decreases the maximum tower-base bending moments for the front-row turbines because the power generation and thrust loads decrease. Concurrently, wake steering increases the maximum tower-base bending moments on the downstream turbines because the power generation and thrust loads increase. A more subtle trend is shown by the darker shades of red for the set of pixels associated with the lowest turbulence intensity. This is because higher freestream turbulence intensity mixes out the wakes more quickly, whereas lower freestream turbulence intensity means the wakes persist further downstream, requiring higher yaw offset angles for wake steering. For the tower-base yaw moment results in Figure 11D, wake steering increases the loads in almost all cases because all turbines are using a nonzero yaw offset. There are a few light-blue pixels for front-row turbines and positive inflow angles that are not well understood.

3.2.2 | Ultimate loads: Extreme events

In the wind turbine design process, the most important ultimate loads are those that define the upper limit of the load envelope. As such, the maximum absolute ultimate load for wake steering and no wake steering results is determined across all inflow conditions and angles for each turbine and QoI. These results are summarized in Table 5 for WT1 and WT2 (a front-row and downstream turbine, respectively), which identify the corresponding inflow condition and inflow angle triggering the ultimate load. When processing the wake steering cases, it is important to recall that not all inflow and wind direction conditions resulted in yaw offsets from the wake steering optimization. Regardless of whether or not yaw offsets were used for a specific case, all inflows and cases were included in the wake steering analysis. The purpose of these tables is to determine which case led to the highest ultimate load for each QoI, and if these results differ when wake steering is present.

TABLE 5 Extreme events table of ultimate loads for each QoI for (a) WT1 and (b) WT2, both with and without wake steering

	(a) WT1										(b) WT2									
	NoSteering	Uinf1	Shear1	TI1	Angle1	Steering	Uinf2	Shear2	TI2	Angle2	NoSteering	Uinf1	Shear1	TI1	Angle1	Steering	Uinf2	Shear2	TI2	Angle2
U-Wind Vel.	26.0183	16.6	0.3	B	8	1	16.6	0.3	B	8	26.3932	16.6	0.3	B	-18	1	16.6	0.3	B	-18
IP Blade Defl.	4.11024	16.6	0.3	B	16	1	16.6	0.3	B	16	4.24804	16.6	0.3	B	0	1	16.6	0.3	B	0
OoP Blade Defl.	19.9691	12.6	0.3	B	20	1.08115	10.6	0.3	B	-2	21.2752	12.6	0.3	B	-2	1	12.6	0.3	B	-2
Shaft Bend.	52677.8	16.6	0.3	B	16	1	16.6	0.3	B	16	51999.5	16.6	0.3	B	2	1	16.6	0.3	B	2
Blade-Root Bend.	86094.2	12.6	0.3	B	18	1.07588	10.6	0.3	B	-2	90720.8	12.6	0.3	B	-2	1	12.6	0.3	B	-2
Blade-Root Pitch.	555.693	10.6	0.3	B	16	1.14359	10.6	0.3	B	-2	830.628	10.6	0.1	B	-4	1.21478	8.6	0.1	D	0
Rot. Speed	8.70016	16.6	0.3	B	16	1	16.6	0.3	B	16	8.85183	12.6	0.3	B	14	1	12.6	0.3	B	14
Shaft Torq.	19904.3	16.6	0.3	B	16	1	16.6	0.3	B	16	19937.3	16.6	0.3	B	18	1	16.6	0.3	B	18
Rot. Thrust	3199.96	12.6	0.3	B	14	1.00583	10.6	0.3	B	-4	3289.19	12.6	0.3	B	-4	1	12.6	0.3	B	-4
Rot. Pwr.	17918.6	16.6	0.3	B	16	1	16.6	0.3	B	16	18223.2	12.6	0.3	B	14	1	12.6	0.3	B	14
Tower-Top Bend.	90957.2	16.6	0.1	B	16	1	16.6	0.1	B	16	91694.1	16.6	0.1	B	10	1	16.6	0.1	B	10
Tower-Top Yaw	39483.4	16.6	0.3	B	16	1	16.6	0.3	B	16	41939.5	16.6	0.3	B	-6	1	16.6	0.3	B	-6
Tower-Base Bend.	340622	12.6	0.3	B	16	1	12.6	0.3	B	16	353817	12.6	0.3	B	-4	1	12.6	0.3	B	-4
Tower-Base Yaw	39482.8	16.6	0.3	B	16	1	16.6	0.3	B	16	41939	16.6	0.3	B	-6	1	16.6	0.3	B	-6
Tower-Top Defl.	0.779865	12.6	0.3	B	6	1	12.6	0.3	B	6	0.823466	12.6	0.3	B	-4	1	12.6	0.3	B	-4
Mud. Bend.	4.95908e+08	12.6	0.3	B	14	1	12.6	0.3	B	14	5.19395e+08	12.6	0.3	B	-4	1	12.6	0.3	B	-4
Mud. Yaw	3.97876e+07	16.6	0.3	B	16	1	16.6	0.3	B	16	4.21643e+07	16.6	0.3	B	-6	1	16.6	0.3	B	-6

Note: No wake steering results (“NoSteering”) are shown as direct values, whereas wake steering results (“Steering”) are shown relative to the no wake steering results for that turbine. If wake steering changed the extreme value by $\pm 1\%$, these cells are colored: blue for the lower value and pink for the higher value. Additionally, the corresponding inflow velocity (“Uinf”), shear exponent (“Shear”), TI class (“TI”), and inflow angle (“Angle”) are identified for each QoI with and without wake steering, with a different color used for each unique value.

Overall, the highest ultimate loads occurred for Class B turbulence with a shear exponent of 0.3 at wind speeds of 12.6 to 16.6 m/s. This makes intuitive sense as this inflow condition represents the highest TI, the highest shear, and highest velocities. This was consistent for all QoI whether or not a turbine was downstream or wake steering was used. The exceptions to this trend occurred for blade-root pitching, with an ultimate condition at rated conditions, and tower-top bending moments, with an ultimate condition at the highest velocity and lower shear exponent. For front-row turbines, the extreme ultimate loads generally occur at higher inflow angles, whereas for downstream turbines they tend to occur at lower inflow angles. This is likely when the turbine is partially waked, which increases the unsteadiness of the inflow and therefore the turbine loads. Additionally, wake steering increased three QoI for the front-row turbine—out-of-plane blade-tip deflection, blade-root bending moment, and blade-root pitching moment—and only one QoI for the downstream turbine, blade-root pitching moment. These results were consistent across all turbines.

When looking at the effects of wake steering on the maximum absolute ultimate loads, for the majority of QoI, the inflow conditions that define the load envelope are those in which no wake steering is applied. Wake steering tended to increase out-of-plane blade deflections, blade-root pitching moments, and blade-root bending moments by more than 1%. This was true for all front-row turbines, and for most downstream turbines. Blade-root pitching moments had the highest increases in ultimate loading, by an average of 12.1% for all turbines and up to 26.5%. To further investigate how wake steering modifies the maximum ultimate loads for all turbines in the wind farm, down-the-row extreme events values are shown in Figure 13 for certain QoI. Figure 13A,B shows the two QoI, blade-root bending and pitching moments,

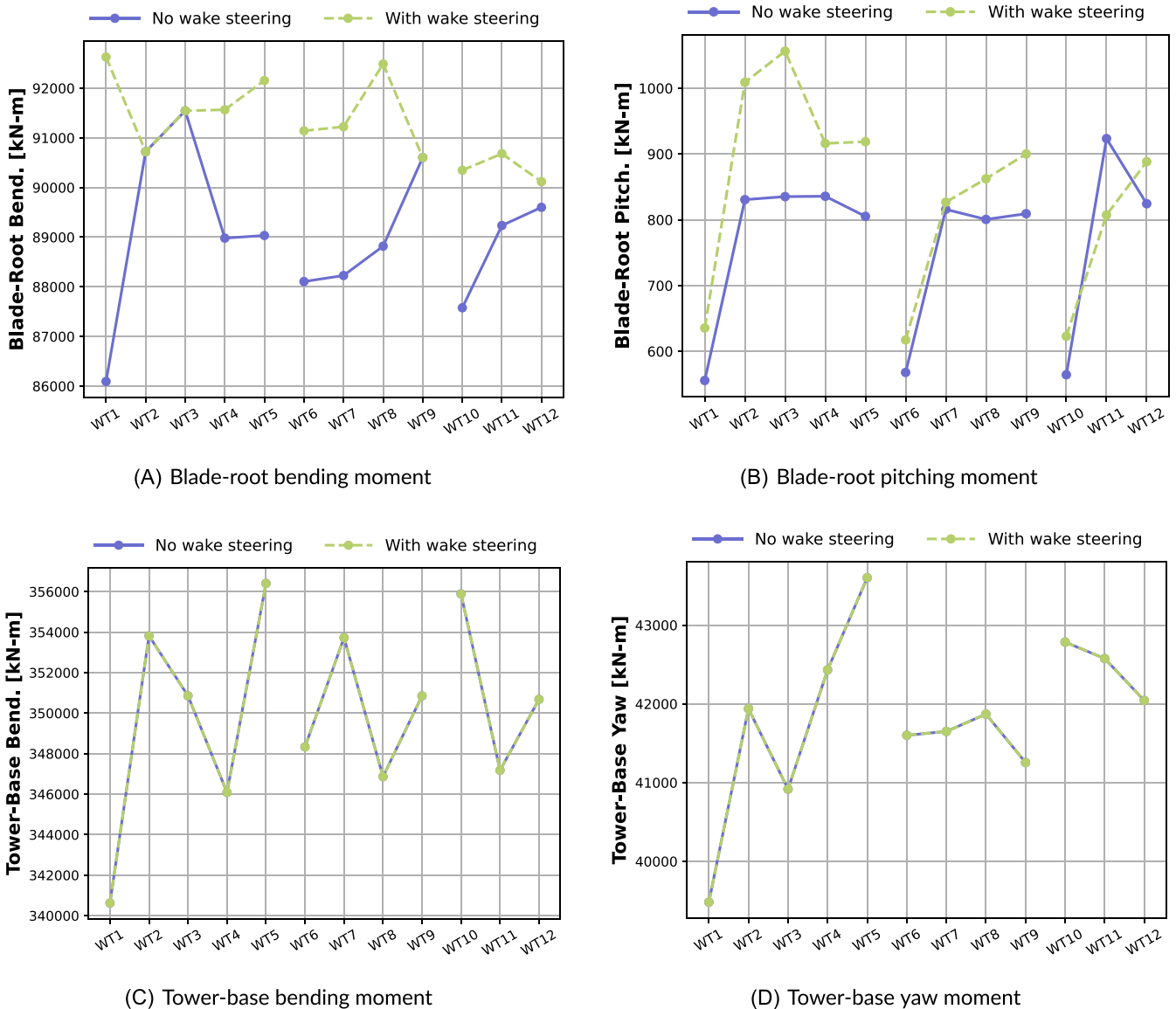


FIGURE 13 Extreme ultimate loads for each turbine, with and without wake steering. Each subplot shows results for a different QoI: (A) Blade-root bending moment, (B) blade-root pitching moment, (C) tower-base bending moment, and (D) tower-base yaw moment

where wake steering increases the maximum absolute ultimate for most of the turbines in the array. For blade-root bending moments in Figure 13A, higher extreme ultimate loads are also more evenly distributed through the array, which could have operational maintenance benefits. However, the maximum absolute blade-root pitching ultimate moments for the downstream turbines exceed those of the front-row turbines even when no wake steering is applied, with the effect exaggerated with wake steering. This is consistent with the hypothesis that partial waking still persists in the simulations and can be a bigger driver of extreme loading than a fully waked scenario. The tower-base extreme ultimate moments in Figure 13C,D are two QoI where there is no difference between the cases with or without wake steering. However, the values through the array are quite noisy and erratic, with no clear trends for front-row or downstream turbines. This behavior implies that the extreme values are not statistically converged and more than six seeds are likely necessary to rigorously determined extreme value trends across the entire wind farm. This also implies that other observations in Figures 5 and 13 could be subject to change if reevaluated with more random seeds.

3.2.3 | Fatigue loads: Short term

Figure 14 shows relative difference pixel plots for each turbine constructed using Equation (4) at each inflow condition and angle combination using short-term DELs. Zoomed-in pixel plots for WT1 and WT2 are shown in Figure 15. Once again, a white cell indicates no change with wake steering, a red cell indicates a higher value with wake steering, and a blue cell indicates a lower value with wake steering.

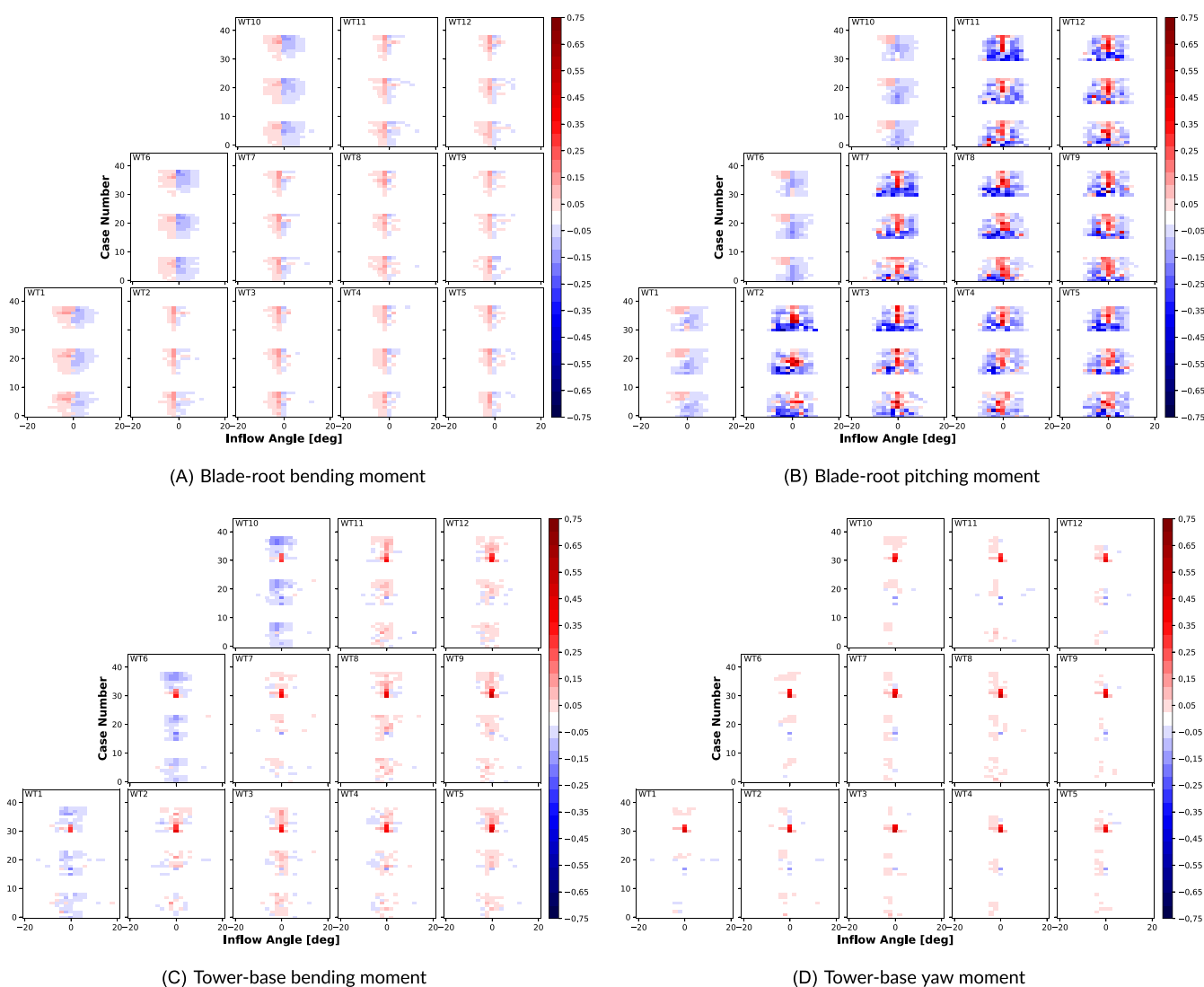


FIGURE 14 Pixel plots of relative difference between short-term fatigue loads for each turbine. Each cell corresponds to a different inflow condition and inflow angle combination. White cells indicate no change with wake steering, red cells indicate a higher value with wake steering, and blue cells indicate a lower value with wake steering

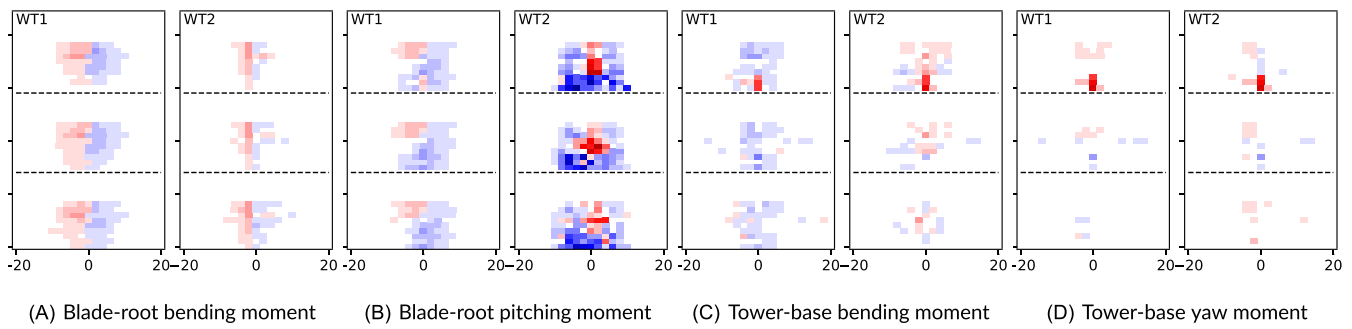


FIGURE 15 Zoomed-in pixel plots of relative difference between short-term fatigue loads for WT1 and WT2. Each cell corresponds to a different inflow condition and inflow angle combination. White cells indicate no change with wake steering, red cells indicate a higher value with wake steering, and blue cells indicate a lower value with wake steering

TABLE 6 Pseudo-lifetime fatigue loads for each QoI for (a, c) WT1 and (b, d) WT2, both with and without wake steering

(a) WT1, all cases			(b) WT2, all cases			(c) WT1, wake steering cases			(d) WT2, wake steering cases		
	NoSteering	Steering		NoSteering	Steering		NoSteering	Steering		NoSteering	Steering
Blade-Root Bend.	36018.4	1.00468	Blade-Root Bend.	36316.4	1.00552	Blade-Root Bend.	33996.7	1.01988	Blade-Root Bend.	33152.9	1.03118
Blade-Root Pitch.	306.606	1.00741	Blade-Root Pitch.	981.67	0.743134	Blade-Root Pitch.	310.716	1.01571	Blade-Root Pitch.	1079.04	0.74311
Shaft Bend.	17294.6	1.00987	Shaft Bend.	16989.7	1.01547	Shaft Bend.	15368.8	1.03898	Shaft Bend.	14606.6	1.0677
Shaft Torq.	1709.15	1.00993	Shaft Torq.	1751.9	0.995336	Shaft Torq.	1839.32	1.01985	Shaft Torq.	1943.44	0.992626
Rot. Thrust	386.748	0.992769	Rot. Thrust	391.729	1.00126	Rot. Thrust	361.214	0.974891	Rot. Thrust	343.901	1.00537
Tower-Top Bend.	11358.8	0.997811	Tower-Top Bend.	11168.7	0.999539	Tower-Top Bend.	10242	0.99146	Tower-Top Bend.	9781.37	0.998231
Tower-Top Yaw	10803.4	1.00109	Tower-Top Yaw	10601.4	1.00139	Tower-Top Yaw	9877.08	1.00421	Tower-Top Yaw	9403.55	1.00591
Tower-Base Bend.	57209.5	0.994248	Tower-Base Bend.	58230.8	1.00204	Tower-Base Bend.	53293.7	0.97987	Tower-Base Bend.	51033.2	1.00874
Tower-Base Yaw	10803.4	1.00109	Tower-Base Yaw	10601.5	1.00139	Tower-Base Yaw	9877.08	1.00422	Tower-Base Yaw	9403.55	1.00591
Mud. Bend.	8.98356e+07	0.994353	Mud. Bend.	9.07788e+07	1.00098	Mud. Bend.	8.27489e+07	0.979501	Mud. Bend.	7.93e+07	1.00438
Mud. Yaw	1.09652e+07	1.00104	Mud. Yaw	1.07649e+07	1.00142	Mud. Yaw	1.0019e+07	1.00405	Mud. Yaw	9.5404e+06	1.00605

Note: The two leftmost tables (a, b) show the results with all cases; the two rightmost tables (c, d) show the results using a subset of the cases where wake steering applies. Results with no wake steering (“NoSteering”) are shown as direct values, whereas results with wake steering (“Steering”) are shown relative to the no-wake-steering results. If wake steering changed the extreme value by $\pm 1\%$, these cells are colored: blue for the lower value and pink for the higher value.

For Figure 14A,B, showing results for blade-root bending moment and blade-root pitching moment, the pixel coloring is quite similar to the ultimate load equivalent plots in Figure 11 and the same comments apply. For Figure 14C,D, showing results for tower-base bending moment and tower-base yaw moment, the colored pixels are far more sparse here than for the ultimate load equivalent plots in Figure 11. The cases where wake steering has increased fatigue loads for the downstream turbines is even more restricted than for ultimate loads; it is more concentrated in the lower velocities, array-aligned inflow angles, and lower turbulence intensity.

3.2.4 | Fatigue loads: Pseudo-lifetime

To create a cumulative fatigue table, the short-term DELs from aggregated individual cases were computed as pseudo-lifetime DELs following the description in Section 2, and shown in Table 6. Pseudo-lifetime DELs were computed for all cases (Table 6 (a, b)), as well as a subset of cases that only included those with wake steering (Table 6 (c, d)).

As was done with ultimate loads, the results from only two turbines are shown here, but all turbines were included in the analysis. When all inflow cases were considered, wake steering had minimal impact on the pseudo-lifetime fatigue loads. In fact, the only QoI that changed by more than 1% was blade-root pitching moment, which was reduced in downstream turbines by an average of 12.7% and up to 18.6%. This null result is due to the frequency with which wake steering is applied. As shown in Figure 5, wake steering is applied at inflow velocities below 12.6 m/s and inflow angles within $\pm 10^\circ$. This accounts for only 31% of the considered cases, thus leading to negligible effects from wake steering when all cases are included in the pseudo-lifetime fatigue analysis. When the pseudo-lifetime fatigue calculations are restricted only to cases where wake steering was applied, as in Table 6 (c, d), the impact of wake steering is more prominent. With this method, several QoI show consistent

TABLE 7 Summary of pseudo-lifetime fatigue loads that change by more than 1% for the subset of cases where wake steering is applied

QoI	No steering higher	Steering higher
Blade-root bending		WT1 & All downstream turbines
Blade-root pitching	All downstream turbines	WT1
Shaft bending		All turbines
Rotor torque	WT4	All front-row turbines
Rotor thrust	All front-row turbines	Some downstream turbines
Tower-base bending	All front-row turbines	Some downstream turbines
Mudline bending	All front-row turbines	Some downstream turbines

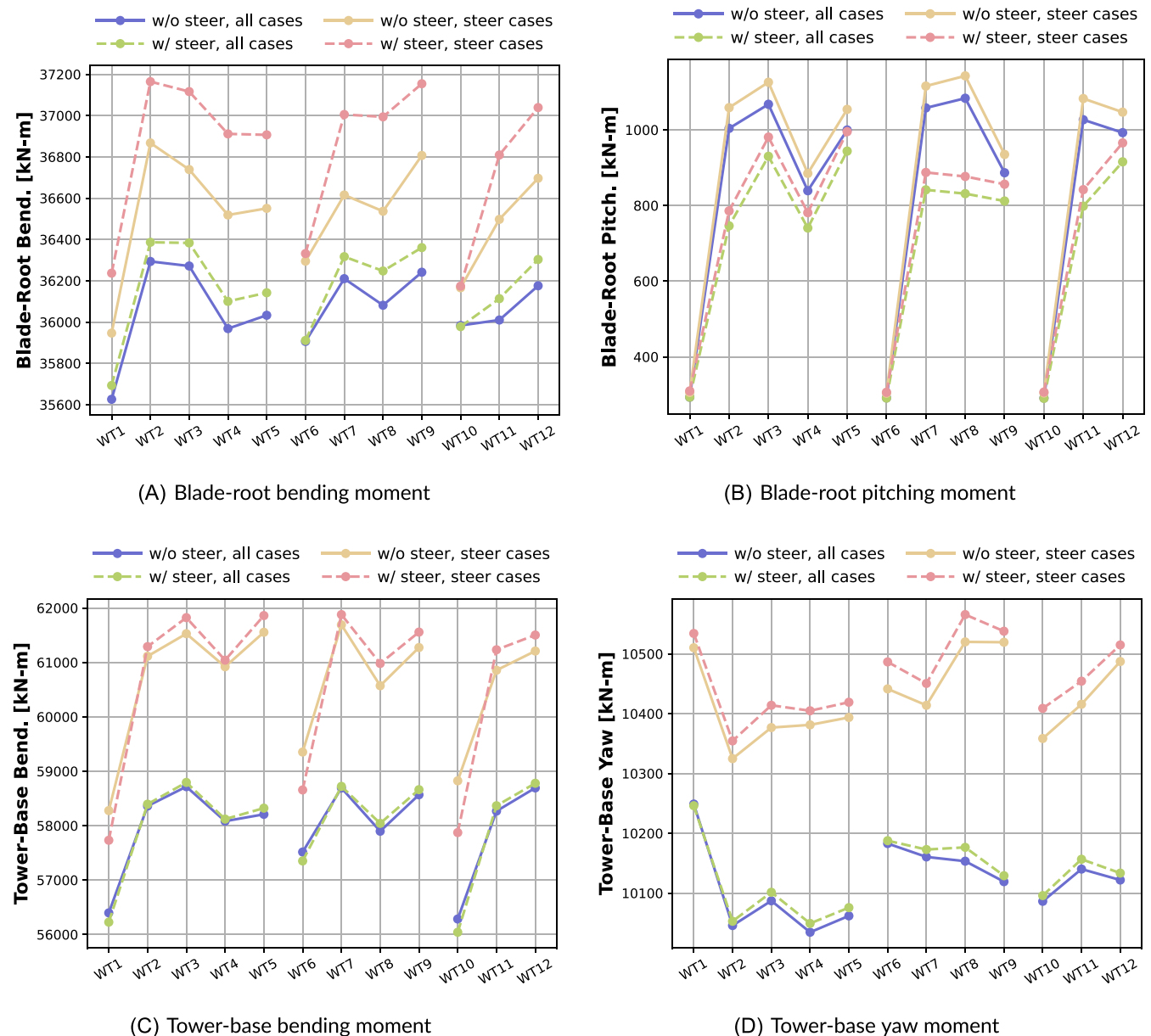


FIGURE 16 Pseudo-lifetime fatigue loads for each turbine, with and without wake steering. Blue and green lines consider all inflow cases whereas red and orange lines only consider cases where wake steering is applied

differences of more than 1% for front-row and downstream turbines. This observation implies that the aggregate impact of wake steering on fatigue load in real-world projects will be dependent on the frequency of wake steering use relative to the higher inflow velocity scenarios that often dominate fatigue damage accumulation, given specific wind farm layout and local conditions. If wake steering is applied infrequently, similar to the 31% of the total case count, there will be a negligible impact on fatigue loads. If wake steering is applied to nearly all wind speeds and directions in the wind rose, then there will be a prominent impact on lifetime fatigue loads. In those sites, the QoI that will be impacted are summarized in Table 7. Further study is needed of an intermediate case, where the wake steering duty cycle is between 60% and 80%, as well as the relative contributions to lifetime fatigue between the wake steering cases and the higher speed inflow cases where wake steering is not used.

The evolution of pseudo-lifetime fatigue loads across the wind farm is shown in Figure 16, enabling a visual comparison of no wake steering versus wake steering. Pseudo-lifetime results of all cases or only cases where wake steering was applied are compared separately. In absolute magnitude, the increases in fatigue loads incurred by using wake steering is smaller than the gap between the case sets where wake steering is used 31% of the time compared to 100% of the time. This implies that cases where wake steering could be used are lower drivers of fatigue, expect for blade-pitching moment. For most of the QoI shown in Figure 16, there is little variation in pseudo-lifetime fatigue damage across the array. To a small degree, the use of wake steering provides a more even fatigue loading distribution for blade-root bending moment in Figure 16A, although it is at a higher level due to increased power production and thrust loads for downstream turbines. Blade-root pitching moment in Figure 16B remains the outlier in that the dominant trends persist with or without wake steering for both sets of cases considered. The higher pitching moment fatigue loads for downstream turbines are alleviated to a small degree by using wake steering. Nevertheless, this QoI is sensitive and dominated to partial waking scenarios that persist in the simulations.

4 | CONCLUSIONS

This study aimed to provide a comprehensive assessment of the loads impact due to wake steering. This included a full-wind-turbine and full-farm perspective of loads, especially the ultimate and fatigue loads that drive design and operational decisions. The IEA Wind 15-MW reference wind turbine²⁴ was chosen to be consistent with the latest commercial available offshore turbine models, and to better understand the loading environment and wake dynamics at this class of turbine rating. While this study looked at a wide variety of inflow conditions and QoIs, there were still many simplifications and assumptions. Therefore, specific recommendations related to wake steering practices are not proposed. Instead, there are a number of key findings that were identified as overarching themes that can be used to inform future wake steering studies and operation:

- For all QoI except the tower or monopile yaw moment, the loads on the first row of turbines significantly decrease with wake steering, resulting in an overall reduction of wind-farm-level peak loads for below and at rated wind speed conditions. The loads on the downstream turbines are closer to those on the front-row turbines, although this is often at a high value for the downstream turbines due to the higher levels of power production and rotor thrust. This is true for all loads statistics—mean, standard deviation, maximum value, and fatigue DEL. This could potentially aid in long-term maintenance planning and strategies by making it easier to schedule maintenance for all turbines at the same time.
- Wake steering increases the yaw moment on the tower and monopile for both front-row and downstream turbines. However, because the tower and monopile typically provide ample yaw stiffness, yaw moments are not usually a design driver or load channel of concern. More investigation for specific tower and monopile designs will be required to ensure that this remains true for the loads imposed by wake steering.
- For specific inflow conditions where wake steering is applied, the maximum value of the load experienced in a time-domain simulation can increase. This is consistent with greater power production and overall thrust loading. However, these scenarios are generally at below-rated conditions that do not define the extreme load envelope that would drive a turbine design.
- Similar to ultimate loads, wake steering can augment fatigue loading cycles for specific inflow scenarios, with blade-root pitching moment observed as the only QoI with significantly lower fatigue. Whether or not this has a measurable impact on total component lifetimes will be dependent on the wake steering “duty cycle” for a given site and also on the relative frequency of higher inflow velocity scenarios in the wind rose that often drive fatigue damage. This is in line with prior findings.^{18,23}
- There is an interplay between wake steering with yaw offsets, especially when considering both positive and negative yaw offsets, and loading asymmetry due to partial waking. Nevertheless, it may also be possible to use wake steering to minimize this effect as the yaw offsets used in this work were derived purely from a power optimization. If the offset angles were chosen with awareness of the load implications, they may be able to nullify this effect.

ACKNOWLEDGEMENTS

This work was authored in part by the National Renewable Energy Laboratory, operated by Alliance for Sustainable Energy, LLC, for the U.S. Department of Energy (DOE) under Contract No. DE-AC36-08GO28308. The views expressed in the article do not necessarily represent the

views of the DOE or the U.S. Government. The U.S. Government retains and the publisher, by accepting the article for publication, acknowledges that the U.S. Government retains a nonexclusive, paid-up, irrevocable, worldwide license to publish or reproduce the published form of this work, or allow others to do so, for U.S. Government purposes. This work was funded by Shell Global Solutions International B.V. under agreement ACT-18-00038-5. The research was performed using computational resources sponsored by the Department of Energy's Office of Energy Efficiency and Renewable Energy and located at the National Renewable Energy Laboratory.

PEER REVIEW

The peer review history for this article is available at <https://publons.com/publon/10.1002/we.2756>.

DATA AVAILABILITY STATEMENT

Due to the large amount of data generated for this work, parts of the data that support the findings of this study may be available from the corresponding author upon reasonable request.

ORCID

Kelsey Shaler  <https://orcid.org/0000-0002-7563-3377>

REFERENCES

- Jiménez Á, Crespo A, Migoya E. Application of a LES technique to characterize the wake deflection of a wind turbine in yaw. *Wind Energy*. 2010;13(6):559-572.
- Fleming PA, Gebraad PMO, Lee S, et al. Evaluating techniques for redirecting turbine wakes using SOWFA. *Renew Energy*. 2014;70:211-218.
- Park J, Kwon S, Law KH. Wind farm power maximization based on a cooperative static game approach. In: Sodano H, ed. *Active and passive smart structures and integrated systems 2013*, Vol. 8688: SPIE; 2013:204-218.
- Gebraad PMO, Teeuwisse FW, van Wingerden JW, et al. Wind plant power optimization through yaw control using a parametric model for wake effects—a CFD simulation study. *Wind Energy*. 2016;19(1):95-114.
- Adaramola MS, Krogstad P-AA. Experimental investigation of wake effects on wind turbine performance. *Renew Energy*. 2011;36(8):2078-2086.
- Medici D, Dahlberg JAA. Potential improvement of wind turbine array efficiency by active wake control (AWC). In: *Proceedings of European Wind Energy Conference The organization; 2003; Madrid, Spain:65-84*.
- Medici D, Alfredsson PH. Measurements on a wind turbine wake: 3D effects and bluff body vortex shedding. *Wind Energy*. 2006;9(3):219-236.
- Wagenaar JW, Machiels L, Schepers J. Controlling wind in ECN's scaled wind farm. *Proc Europe Premier Wind Energy Event*. 2012;1(1):685-694.
- Fleming P, Annoni J, Shah JJ, et al. Field test of wake steering at an offshore wind farm. *Wind Energy Sci*. 2017;2(1):229-239.
- Fleming P, King J, Dykes K, et al. Initial results from a field campaign of wake steering applied at a commercial wind farm—part 1. *Wind Energy Sci*. 2019;4(2):273-285. <https://wes.copernicus.org/articles/4/273/2019/>
- Fleming P, King J, Simley E, et al. Continued results from a field campaign of wake steering applied at a commercial wind farm—part 2. *Wind Energy Sci*. 2020;5(3):945-958. <https://wes.copernicus.org/articles/5/945/2020/>
- Doekemeijer BM, Kern S, Maturu S, et al. Field experiment for open-loop yaw-based wake steering at a commercial onshore wind farm in Italy. *Wind Energy Sci Discuss*. 2020;2020:1-22.
- Houck DR. Review of wake management techniques for wind turbines. *Wind Energy*. 2021;25(2):195-220.
- Thomsen K, Sørensen P. Fatigue loads for wind turbines operating in wakes. *J Wind Eng Industr Aerodyn*. 1999;80(1):121-136.
- Meng H, Lien F-S, Glinka G, Li L, Zhang J. Study on wake-induced fatigue on wind turbine blade based on elastic actuator line model and two-dimensional finite element model. *Wind Eng*. 2019;43(1):64-82.
- Damiani R, Dana S, Annoni J, et al. Assessment of wind turbine component loads under yaw-offset conditions. *Wind Energy Sci*. 2018;3(1):173-189.
- Zalkind DS, Pao LY. The fatigue loading effects of yaw control for wind plants. In: 2016 American Control Conference (ACC) IEEE; 2016:537-542.
- Ennis BL, White JR, Paquette JA. Wind turbine blade load characterization under yaw offset at the Swift facility. *Journal of physics: Conference series*, Vol. 1037: IOP Publishing; 2018:52001.
- Shaler K, Debnath M, Jonkman J. Validation of FAST.farm against full-scale turbine SCADA data for a small wind farm. *Journal of Physics: Conference Series*, Vol. 1618: IOP Publishing; 2020:62061.
- Ciri U, Rotea MA, Leonardi S. Effect of the turbine scale on yaw control. *Wind Energy*. 2018;21(12):1395-1405.
- Bartl J, Mühle F, Sætran L. Wind tunnel study on power output and yaw moments for two yaw-controlled model wind turbines. *Wind Energy Sci*. 2018;3(2):489-502.
- Urbán AM, Larsen TJ, Larsen GC, Held DP, Dellwik E, Verelst D. Optimal yaw strategy for optimized power and load in various wake situations. *Journal of physics: Conference series*, Vol. 1102: IOP Publishing; 2018:12019.
- Kanev S, Bot E, Giles J. Wind farm loads under wake redirection control. *Energies*. 2020;13(16):4088.
- Gaertner E, Rinker J, Sethuraman L, et al. Definition of the IEA 15-megawatt offshore reference wind turbine. Tech. Rep. NREL/TP-5000-75698, Golden, CO, National Renewable Energy Laboratory; 2020.
- Jonkman J, Shaler K. Fast.farm user's guide and theory manual. Tech. Rep. NREL/TP-5000-78485, Golden, CO, National Renewable Energy Laboratory; 2021.
- Openfast documentation. <https://openfast.readthedocs.io/en/master/>; 2017.
- Larsen GC, Madsen HA, Thomsen K, et al. Wake meander: A pragmatic approach. *Wind Energy*. 2008;11:337-95.
- Kretschmer M, Jonkman J, Pettas V, Cheng PW. Fast.farm load validation for single wake situations at alpha ventus. *Wind Energy Sci*. 2021;6:1247-1262.

29. Doubrawa P, Annoni J, Jonkman J, Ghate A. Optimization-based calibration of FAST.Farm parameters against SOWFA. In: 36th Wind Energy Symposium. AIAA Scitech Forum AIAA; 2018; Kissimmee, FL.
30. Jonkman J, Doubrawa P, Hamilton N, Annoni J, Fleming P. Validation of FAST.farm against large-eddy simulations. *Journal of physics: Conference series*, TORQUE 2018, vol. 1037. Milano, Italy: EAWWE; 2018:62005.
31. 61400-3-1 I. Wind energy generation systems - part 3-1: Design requirements for fixed offshore wind turbines, 1st ed. Tech. Rep., Geneva, Switzerland, International Electrotechnical Commission; 2019.
32. Jonkman B. Turbsim user's guide v2.00.00. Tech. Rep. NREL/TP, Golden, CO, National Renewable Energy Laboratory; 2014.
33. Shaler K, Jonkman J, Hamilton N. Effects of inflow spatiotemporal discretization on wake meandering and turbine structural response using fast.farm. *J Phys: Conf Ser*. 2019;1256:12023.
34. Floris documentation. <https://floris.readthedocs.io/en/documentation/>; 2019.
35. Hayman GJ. Mlife theory manual for version 1.00. Tech. Rep. NREL/TP, Golden, CO, National Renewable Energy Laboratory; 2012.
36. Stanley APJ, King J, Bay C, Ning A. A model to calculate fatigue damage caused by partial waking during wind farm optimization. *Wind Energy Sci Discuss*. 2020;2020:1-34.

How to cite this article: Shaler K, Jonkman J, Barter GE, Kreeft JJ, Muller JP. Loads assessment of a fixed-bottom offshore wind farm with wake steering. *Wind Energy*. 2022;25(9):1530-1554. doi:10.1002/we.2756

APPENDIX A: FAST.Farm CALIBRATION RESULTS

SOWFA, a large-eddy simulation computational fluid dynamics code, was used to calibrate FAST.Farm wake parameters for simulating the 15-MW IEA Wind Reference Wind Turbine. The test case is shown in Figure A1(A), with three turbines aligned to the inflow, spaced seven rotor diameters apart. The first turbine (WT1) yaw offset was set to either 0° or 25° , the second turbine (WT2) was 0° or 20° , and the third turbine (WT3) was fixed at 0° yaw. The freestream turbulence intensity was either 6% (low-TI case) or 10% (high-TI case). FAST.Farm and SOWFA were compared using the underlying time-series and also the overall probability distributions of the rotor power, rotor torque, rotor speed, and wake deflection for the test matrix.

In the baseline cases with no yaw offset, there was good agreement between SOWFA and FAST.Farm predictions for all QoI and both TI values, especially for WT1. Further downstream at WT3, the match between SOWFA and FAST.Farm is not as close, but this is due to known shortcomings in FAST.Farm with regards to additive wake superposition. However, for the cases with turbine yaw offset, more differences were seen for all QoI and all turbines, which is depicted in Figure A2. Because the discrepancies occurred only when turbine yaw was present, they were determined to be caused by the use of FAST.Farm parameters relating to horizontal wake deflection correction for larger turbine ratings and diameters that are not ideal for the 15-MW IEA Wind Reference Wind Turbine.

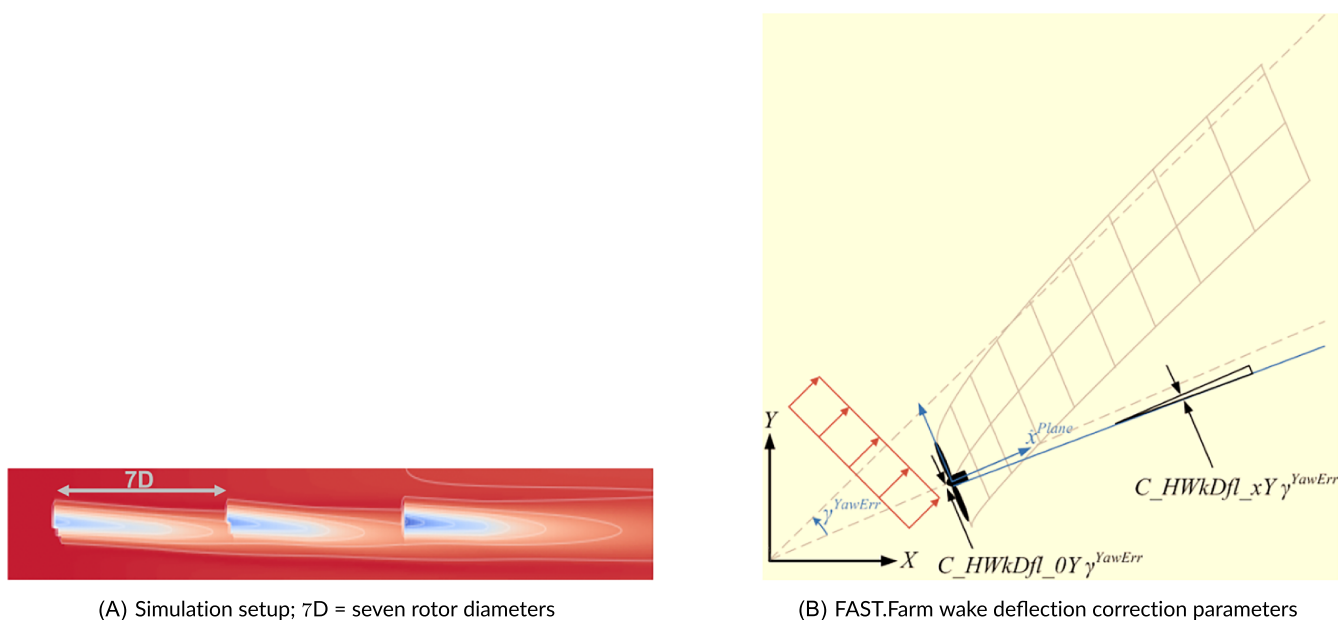


FIGURE A1 Simulation setup for calibration against SOWFA and the FAST.Farm parameters that were tuned for improved tuning for the IEA Wind 15-MW reference turbine

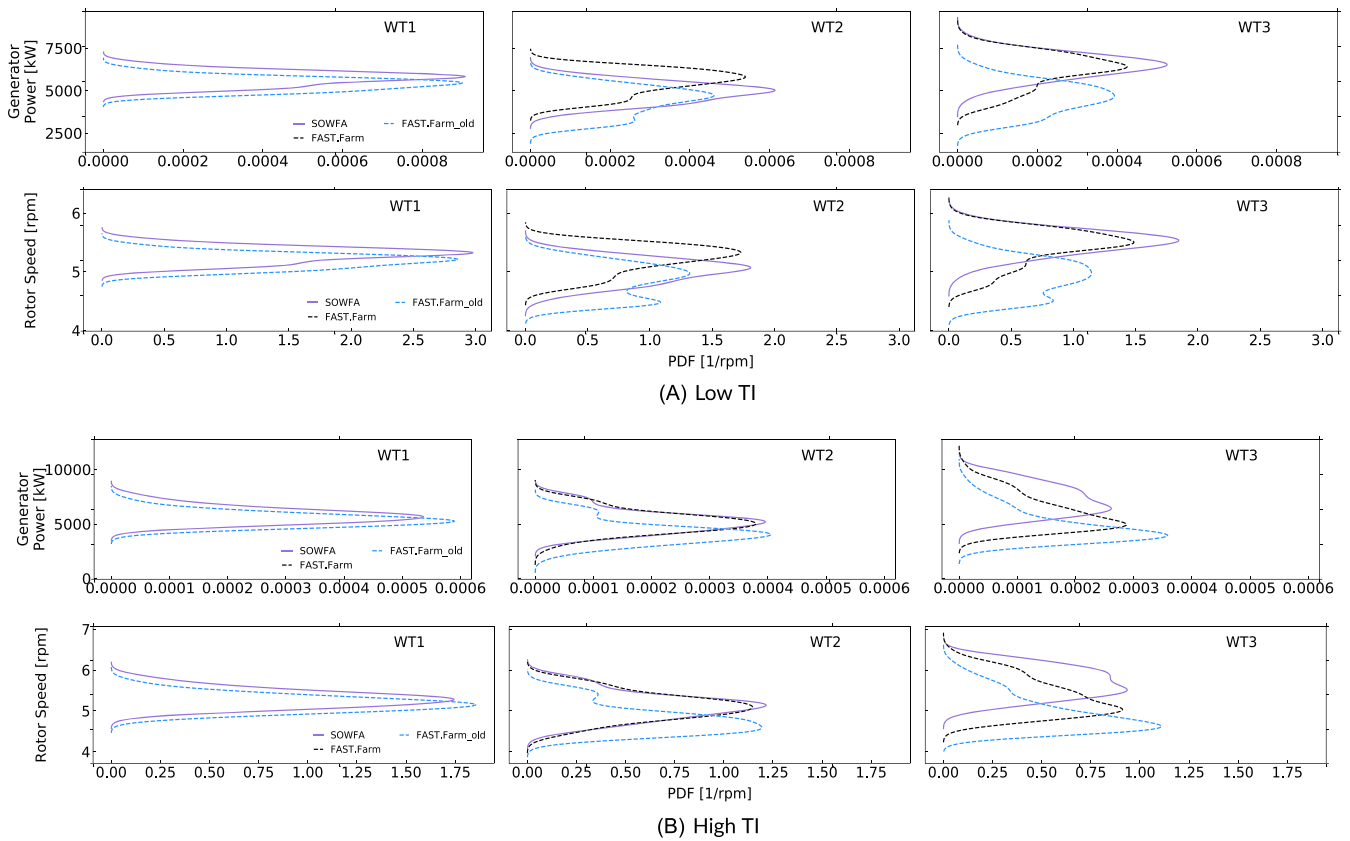


FIGURE A2 Probability density function (PDF) of generator power and rotor speed comparing SOWFA results (purple lines) with precalibration FAST.Farm results (blue dashed lines) and postcalibration FAST.Farm results (black dashed lines) for all turbines. Cases show results for WT1, WT2, and WT3 yawed at 25°, 20°, and 0°, respectively, with (A) low-TI and (B) high-TI inflow

The FAST.Farm wake deflection correction model geometry is shown in Figure A1(B). There are two parameters related to horizontal wake deflection: C_{HWkDf1_OY} and C_{HWkDf1_xY} . C_{HWkDf1_OY} [m/deg] describes the offset from the dashed turbine centerline to the solid line at the rotor plane, and C_{HWkDf1_xY} [1/deg] describes the slope of the solid line relative to the rotor axis. The parameters were calibrated using a grid search and optimization that focused on the wake deflection and power generation of the downstream turbines, WT2 and WT3. The wake deflection and power generation were expressed as percentage errors between FAST.Farm and SOWFA,

$$\Delta \bar{y}_{off} = \frac{\|\bar{y}_{off,FF} - \bar{y}_{off,S}\|}{\|\bar{y}_{off,S}\|} \quad (A1)$$

$$\Delta \bar{P} = \frac{\|\bar{P}_{FF} - \bar{P}_S\|}{\|\bar{P}_S\|} \quad (A2)$$

where y_{off} is the average wake offset, P is the power generation, the subscripts FF and S denote FAST.Farm and SOWFA, respectively, and the $\|x\|$ -notation is the standard norm of the time series. Error measures from both downstream turbines and multiple cases were combined into a single summary error measure.

For the optimization over all simulations, metrics, and turbines, the minimum error parameter values were sensitive only to C_{HWkDf1_xY} , with an optimal value of -0.002 (compared to a default value of -0.004). There was negligible change with varying C_{HWkDf1_OY} , so the default value of 0.3 was unchanged from past FAST.Farm calibration efforts.

Figure A2 contrasts the simulations from FAST.Farm both before and after the recalibration against the SOWFA “reference” results. The postcalibration FAST.Farm results (black dashed line) match the SOWFA results (purple line) better for WT2 and WT3 in all QoI than the precalibration FAST.Farm results (blue dashed line). The improved calibration was deemed sufficient to proceed with the larger wake steering loads study.

APPENDIX B: SPATIAL VARIATION OF TEMPORAL VARIANCE

The standard deviation of the wind field over time varies spatially even when the turbulence class is the same. This is partly a product of TurbSim generating turbulent flowfields with the specified spatial coherence, which means the target standard deviation value is satisfied in aggregate, but not at every point in the field. An example of this is shown in Figure B1 for Class C turbulence and a shear exponent of 0.2 over various wind speeds. The spatial variability of turbulence does lead to some random inconsistencies in inflow conditions between turbines in the array, which can be seen in some load channels that are not otherwise dominated by turbine operations, especially in the nonzero inflow angle results. Using more random seeds could lessen the impact of these inconsistencies. Six seeds were used in this work following IEC conventions. The same seeds are used for both without and with wake steering simulations to not bias the comparison.

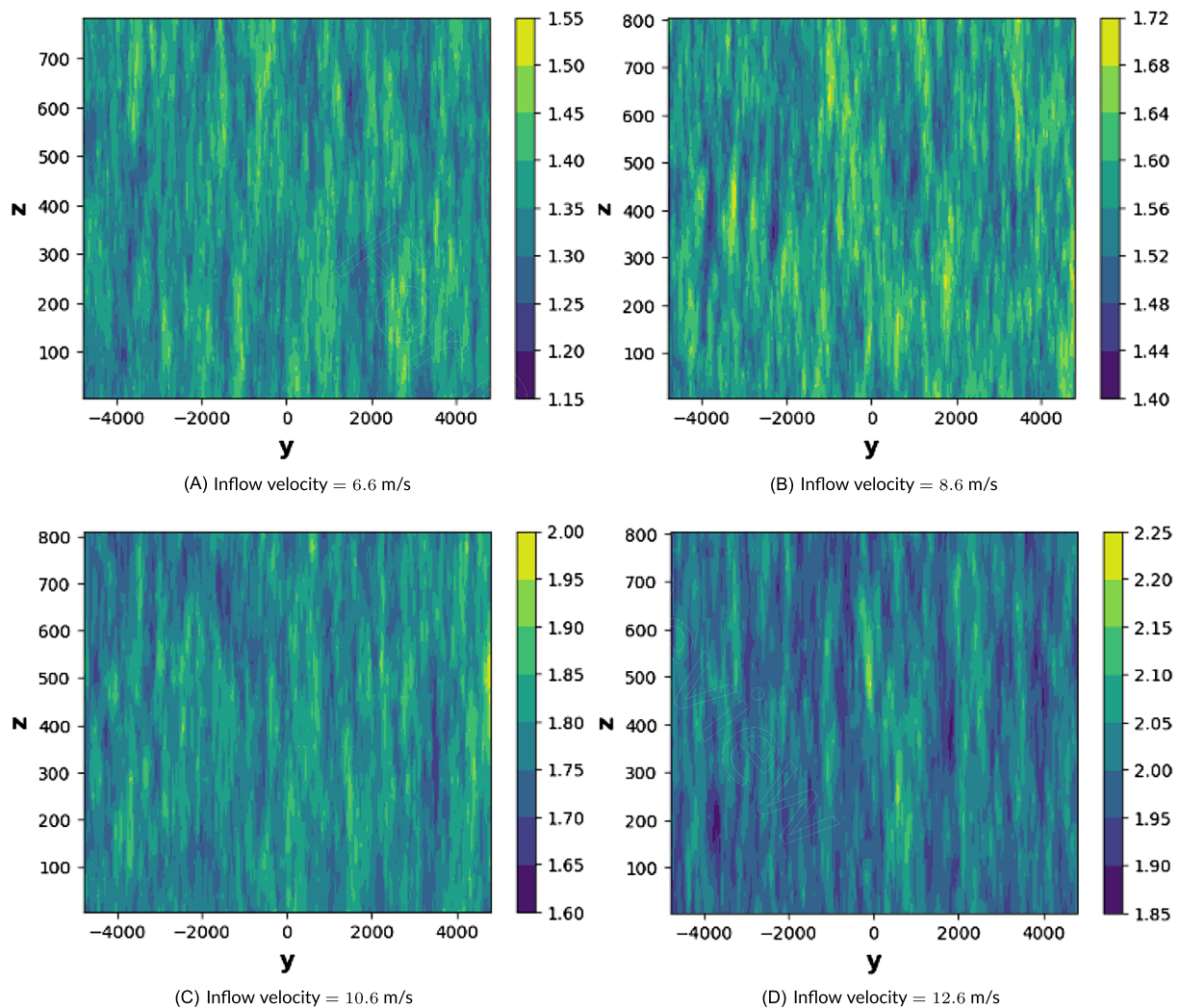


FIGURE B1 Standard deviation of u-direction inflow velocity in [m/s] over the simulation time in the y-z plane demonstrating spatial variability of turbulence. All results are for Class C turbulence with a shear exponent of 0.2